Université du Québec
à Rimouski

Étude de la répartition des espèces soufrées dans les sédiments de l'estuaire maritime du Saint-Laurent

Mémoire présenté

dans le cadre du programme de maîtrise en océanographie

en vue de l'obtention du grade de maître ès sciences (M.Sc.)

PAR

© GWENN DUVAL

Mai 2025

Composition du jury :

Jean-Carlos Montero-Serrano, président du jury, UQAR-ISMER

André Pellerin, directeur de recherche, UQAR-ISMER

Gwénaëlle Chaillou, codirectrice de recherche, UQAR-ISMER

Alfonso Mucci, codirecteur de recherche, Université McGill

Alexander Michaud, examinateur externe, Ohio State University

Dépôt initial le 29 janvier 2025 Dépôt final le 23 mai 2025

« Les mondes océaniques pourront-ils demeurer les cristallisoirs de la vie en marche ? Ou bien seront-ils les derniers égouts d'alchimismes incontrôlés ? » - Anita CONTI

REMERCIEMENTS

L'Océan est bien vaste pour les esprits curieux. Ce mémoire de maîtrise en océanographie, rêve de femme marin voguant avec l'âme pleine de questions, vient compléter un audacieux retour aux études. Le parcours m'a appris des centaines de choses et m'a fait découvrir l'ampleur des moyens qu'emploie la communauté scientifique pour tenter de préserver ce qu'il nous reste de nature.

Je remercie André, mon directeur de maîtrise, qui m'a donné la chance d'entrer dans le monde de l'océanographie. Je le remercie pour la science qu'il m'a transmise mais surtout pour la confiance qu'il m'a accordée en me laissant mener mes projets parallèles. C'était d'abord une déception que les terrains et échanges internationaux n'aient pas lieu, mais c'est devenu l'occasion pour moi de monter *Continuum Océan*, un projet de collecte de données à la voile, ainsi que de participer à la *Transat Québec-Saint-Malo 2024* en tant que co-skipper. Merci donc d'avoir compris mon besoin d'aventure lorsqu'il a dépassé le cadre académique.

Merci à Gwénaëlle Chaillou et à Alfonso Mucci pour leurs commentaires pertinents sur mes résultats et ma rédaction ainsi que pour leur soutient.

Merci à mes amis de la Marina de Rimouski : Myriam, Enora, Paul, Nico, Delphine, Marie et Martin. Entre les vagues, les randonnées, les soupers, les grands dilemmes et les sorties de ski dans les bois, les moments partagés ont rendu la vie belle. Merci au Club de Trail qui m'a motivée, hiver comme été, à courir dans la forêt, spécialement à Catherine, Roxane, Corine et Amélie. Merci à mes amis Valentin et Talia, pour les sorties aux oiseaux et leur écoute bienveillante. Merci aussi à tous ceux qui ont partagé l'aventure de *Continuum Océan*. Merci à mes parents, à Max et Viv', à Baba et Deda. Merci spécial à Sanja et à Ghislaine, pour leur soutien indéfectible, même à distance, dans les moments plus laborieux.

Et merci à Louise, pour ce qu'elle m'insuffle depuis toujours.

RÉSUMÉ

Trois carottes de sédiments ont été prélevées dans le Chenal Laurentien, dans l'estuaire maritime du Saint-Laurent (LSLE *pour Lower St. Lawrence Estuary*), entre Rimouski et Baie-Comeau, en mai 2023, afin d'identifier les facteurs qui contrôlent la distribution des espèces soufrées dans ces sédiments riches en fer en contexte d'hypoxie persistante. Il est attendu que la désoxygénation progressive des eaux profondes depuis 1930 modifie le cycle sédimentaire du soufre en augmentant le taux de sulfato-réduction (catabolisme anaérobie de la matière organique sédimentaire) et la production de sulfure d'hydrogène ($\sum H_2S$). Toutefois, les concentrations élevées en fer solide réactif (>200 µmol/g) entraînent une précipitation rapide du $\sum H_2S$ sous forme de sulfures acides volatils (AVS pour Acid Volatile Sulfides). Le $\sum H_2S$ ne s'accumule donc pas dans les eaux interstitielles. Dans un tel environnement, la conversion des AVS en pyrite dépend principalement de l'oxydation du soufre réduit (S(-II)) en espèces soufrées ayant des degrés d'oxydation intermédiaires, dont le soufre élémentaire (S(0)) et les polysulfures (S_n(-II)). Les rapports AVS sur pyrite varient significativement entre les trois stations, malgré des taux de sulfato-réduction similaires. Aux stations en amont, les taux de sédimentation légèrement plus élevés sont associés à des concentrations plus importantes d'AVS (jusqu'à ~30 µmol/g), mais leur conversion en pyrite est inhibée. En revanche, à la station en aval, où les taux de sédimentation sont plus faibles, les concentrations en AVS sont aussi plus faibles (< 5 µmol/g) et leur conversion en pyrite semble favorisée. Ces différences reflètent les effets combinés du taux de sédimentation et de l'oxygénation des eaux de fond, qui modulent l'oxydation du $\sum H_2S$ et des AVS ainsi que la conversion de ces derniers en pyrite. Ainsi, à des taux de sédimentation plus élevés, les AVS sont plus rapidement enfouis sous l'interface eau-sédiment, les isolant des oxydants nécessaires à la formation de polysulfures ; la formation de pyrite est alors inhibée. Nos résultats soulignent l'importance de la dynamique sédimentaire dans le cycle diagenétique du soufre, particulièrement sous des conditions hypoxiques. L'hypoxie compresse la suite des réactions redox plus près de l'interface eau-sédiment et altère la contribution relative des réactions cataboliques à l'oxydation de la matière organique qui s'accumule dans les sédiments du LSLE, mais l'abondance de fer réactif profère un tampon contre l'accumulation et la diffusion de $\sum H_2S$ dans les eaux interstitielles, atténuant les impacts écologiques potentiels. Établir la résilience du cycle du soufre face à la désoxygénation en cours est essentiel pour comprendre les implications plus larges des changements environnementaux dans le LSLE.

Mots clés : Hypoxie, Cycle du soufre, sulfures acides volatils (AVS), Pyrite, Sulfato-réduction, Fer réactif, Processus de réoxydation, Sédiments du chenal laurentien

ABSTRACT

Three sediment cores were recovered in the Laurentian Trough along the Lower St. Lawrence Estuary (LSLE) between Rimouski and Baie-Comeau in May 2023, to elucidate factors that control the distribution of sulfur species in these iron-rich sediments under persistent bottom-water hypoxia. We anticipated that ongoing bottom-water deoxygenation since 1930 would alter the sedimentary sulfur cycle by increasing the sulfate reduction rate (anaerobic catabolism of organic matter) and hydrogen sulfide ($\sum H_2S$) production. In the presence of elevated solid reactive iron concentrations (>200 µmol/g), however, the $\sum H_2S$, generated by sulfate reduction, is rapidly sequestered as acid-volatile sulfides (AVS) and does not accumulate in the porewaters. Under these conditions, the conversion of AVS to pyrite depends mostly on the oxidation of reduced sulfur (S(-II)) to intermediate redox species such as elemental sulfur (S(0)) and polysulfides (S_n(-II). Despite similar sulfate-reduction rates at the three stations, the AVS-to-pyrite ratio varies significantly. At the upstream stations, higher sedimentation rates are associated with greater AVS concentrations (up to ~30 µmol/g) but their conversion to pyrite is inhibited. In contrast, at the downstream station, where sedimentation rates are lower, AVS concentrations were also lower (>5 µmol/g) and their conversion to pyrite was presumably more efficient. These differences reflect the combined effects of the sedimentation rate and bottom-water oxygenation that modulate the extent of $\sum H_2S$ and AVS oxidation and the conversion of the latter to pyrite. Hence, at higher sedimentation rates, AVS is rapidly buried below the sediment-water interface, distancing it from oxidants and inhibiting pyrite formation. Our findings underscore the importance of sedimentation dynamics in shaping the diagenetic sulfur cycle under hypoxic conditions. Whereas bottom-water hypoxia has compressed the suite of catabolic redox reactions in the LSLE sediments and altered their relative contribution to the remineralization of organic matter, the abundance of solid reactive iron provides a buffer against porewater $\sum H_2S$ accumulation and diffusion, mitigating potential ecological impacts. Establishing the resilience of sulfur cycling to ongoing deoxygenation is essential for understanding the broader implications of environmental change in the LSLE.

Keywords: Hypoxia, Sulfur cycle, Acid-volatile sulfides (AVS), pyrite, sulfate reduction, reactive iron, reoxidation processes, Laurentian Trough sediments

TABLE DES MATIÈRES

LISTE DES TABLEAUX

LISTE DES FIGURES

LISTE DES ABRÉVIATIONS, DES SIGLES ET DES ACRONYMES

LSLE	Lower St.Lawrence Estuary
GSL	Gulf of St. Lawrence
AVS	Acid Volatile Sulfide
CRS	Chromium reducible Sulfur
C_{org}	Organic carbon
ODP	oxygen penetration depth
SWI	Sediment-water interface
SAR	Sediment accumulation rate
SR	Sulfate reduction
SRR	Sulfate reduction rate

INTRODUCTION GÉNÉRALE

Hypoxie et cycle du soufre sédimentaire

L'équilibre de nos écosystèmes repose en partie sur des suites de réactions chimiques interdépendantes, mais les impacts anthropiques mènent à l'altération des cycles naturels de certains éléments et viennent à bousculer ces réactions. Certains éléments, jusqu'alors enfouis dans les sédiments, peuvent être libérés sous forme toxique (Luther et al., 2004; Duan et al., 2021). C'est le cas du soufre, dont le cycle biogéochimique sédimentaire en milieu marin est dépendant de la concentration en oxygène dissous dans les eaux profondes. Or, les concentrations en oxygène dans les eaux surnageantes, particulièrement en milieu côtier, sont en proie à un phénomène de désoxygénation à l'échelle mondiale (Diaz et Rosenberg, 1995, 2008; Falkowski et al., 2011; Breitburg et al., 2018; Fredriksson et al., 2024). Ce phénomène, lié en partie au réchauffement des océans et à l'eutrophisation en région côtière, est alarmant (Diaz, 2001; Rabalais et al., 2009; Keeling et al., 2010; Breitburg et al., 2018).

On dénote à l'heure actuelle plus de 500 sites hypoxiques en milieux côtiers et estuariens, où les concentrations en oxygène dissous dans les eaux profondes sont inférieures au seuil de 62 µmol/L (Fig. 1 : Breitburg et al., 2018). L'oxygène est nécessaire à la respiration des organismes vivants, mais joue aussi un rôle fondamental dans la reminéralisation de la matière organique. La consommation de l'oxygène dissous dans les eaux profondes d'une colonne d'eau stratifiée et dans les sédiments par la reminéralisation de la matière organique peut diminuer sa concentration jusqu'à atteindre, dans certains cas, son épuisement, on parle alors d'anoxie (Diaz, 2001; Rabalais et al., 2009).

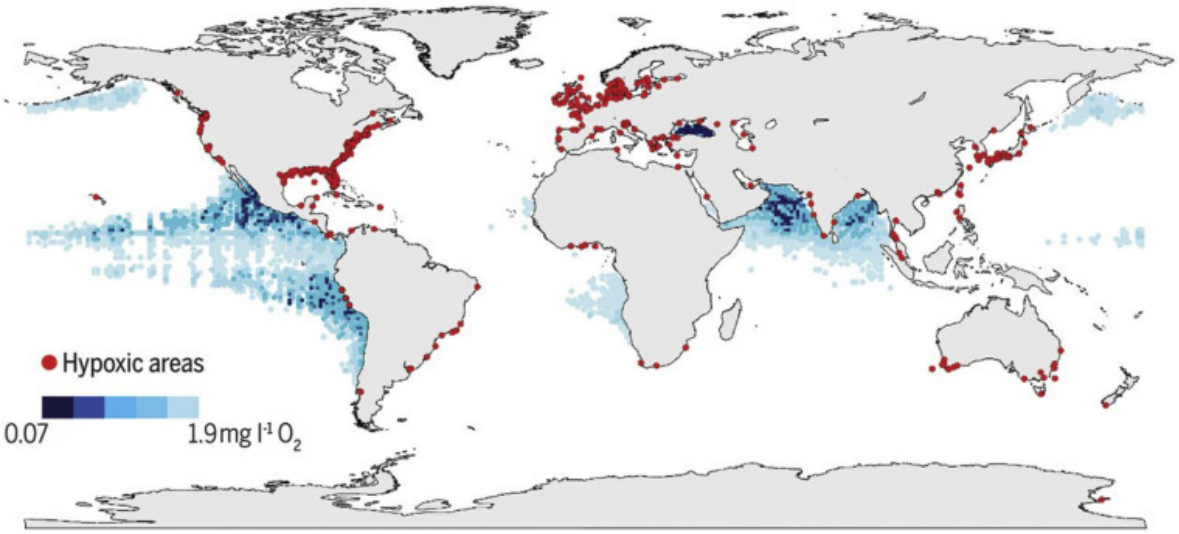

Figure 1. Concentrations d'oxygène dans les mers et l'océan et désoxygénation des eaux côtières (<30 km des côtes). Les points rouges représentent les zones côtières où des concentrations en oxygène dissous inférieures au seuil de l'hypoxie (62,5 µmol/L) ont été observées depuis 1960 (Tiré de Breitburg et al., 2018)

Les zones côtières et estuariennes sont les sites de nombreux échanges biogéochimiques : la proximité des terres entraîne un apport de nutriments issus du lessivage des sols, de polluants industriels et de déchets liés aux autres activités humaines. Leur productivité élevée en fait des acteurs majeurs de l'enfouissement et de la reminéralisation de la matière organique, des composantes importantes mais souvent négligées du cycle global du carbone (Bauer et al., 2013; Regnier et al., 2022). Ce cycle, fondamental pour la régulation du climat, repose sur une série de réactions d'oxydo-réduction parmi lesquels la sulfato-réduction, ou l'oxydation microbienne de la matière organique par les sulfates, occupe une place centrale (Jørgensen, 1982).

Lors de la sulfato-réduction, le S (+VI) des sulfates sert d'oxydant pour la dégradation de la matière organique dans les environnements anoxiques. Produit naturel de la sulfato-réduction, le sulfure d'hydrogène ($\sum H_2S$: H_2S et HS^-) est une espèce toxique qui est

habituellement piégé dans les sédiments sous forme de sulfures de fer ou réoxydé sous forme de sulfates en présence d'oxygène ou d'autres oxydants. Or, lorsqu'il y a un appauvrissement de la concentration en oxygène dissous dans les eaux profondes ou une augmentation de l'apport en matière organique aux sédiments, l'équilibre du cycle du soufre sédimentaire est perturbé (Katsev et al., 2007; Middelburg and Levin, 2009). Ces conditions peuvent mener à une accumulation de $\sum H_2S$ dans les eaux porales, sa diffusion vers les eaux surnageantes et, ultimement, son relargage dans la colonne d'eau lorsque les concentrations en oxygène dissous des eaux surnageantes sont nulle (Luther et al., 2004).

Pour mieux comprendre les réponses biogéochimiques à la désoxygénation des eaux profondes, il est important d'étudier les micro-dynamiques du cycle du soufre dans des environnements spécifiques. Un terrain d'étude tout désigné pour ce travail est le chenal laurentien, situé dans l'estuaire maritime du Saint-Laurent (LSLE, pour *Lower St. Lawrence Esturary*). Cet environnement estuarien se distingue par son abondance en fer réactif (Gagnon et al., 1995, 1996; Katsev et al., 2007; Lefort et al., 2012) et son exposition à une désoxygénation persistante depuis plusieurs décennies (Gilbert et al., 2005; Jutras et al., 2020, 2023a). Ces caractéristiques en font un laboratoire naturel idéal pour explorer les interactions complexes entre le cycle du soufre, la matière organique et les conditions d'oxygénation des eaux profondes (Fig. 2).

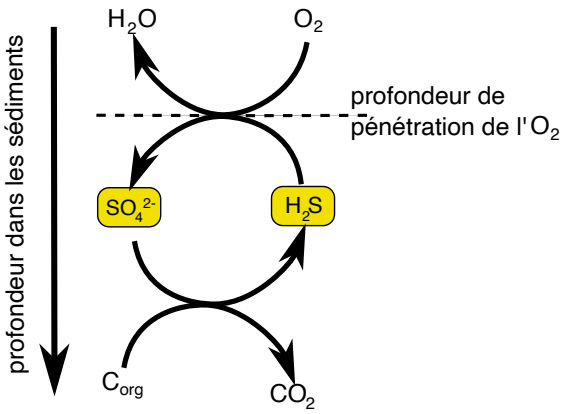

Figure 2. Modèle conceptuel simplifié du couplage de l'utilisation des sulfates pour la respiration du carbone organique et l'oxydation des sulfures par l'oxygène (d'après Aller (1994) et Middelburg (2019))

Hypoxie dans l'estuaire maritime du Saint-Laurent

Le système hydrographique du Saint-Laurent joint les Grands Lacs à l'océan Atlantique et comporte une portion fluviale, une portion estuarienne et un golfe (Fig. 3). L'estuaire maritime du Saint Laurent fait la jonction entre l'estuaire moyen et le golfe. Le chenal laurentien est la principale caractéristique bathymétrique de l'estuaire maritime et du golfe du Saint-Laurent (El-Sabh et Silverberg, 1990). Il s'agit d'une vallée sous-marine de 250 à 350 mètres de profondeur creusée par l'érosion glaciaire du quartenaire (King et Maclean, 1970) qui s'étend du bord du plateau continental nord-américain jusqu'à Tadoussac, où un important seuil d'environ 20 m marque la tête du chenal (Belzile et al., 2016). Les eaux de l'estuaire maritime sont fortement stratifiées thermiquement, et tout au long de l'année. En l'absence de glace, on distingue trois couches qui caractérisent la circulation estuarienne. Les eaux de surface, peu salées, s'écoulent vers l'océan Atlantique. En dessous, la couche intermédiaire froide, formée en hiver dans le golfe ainsi que les eaux profondes, salées, qui proviennent de l'océan Atlantique par le détroit de Cabot, migrent vers la tête du chenal (Gilbert et al., 2005 ; Stevens et al., 2024). Les eaux profondes qui entrent

par le détroit de Cabot sont constituées d'un mélange des eaux froides et riches en oxygène issues du courant du Labrador et des eaux chaudes et appauvries en oxygène dissous du Gulf Stream. Migrant à une vitesse d'environ 0.5 cm s^{-1}, elles mettent de 2 à 5 ans pour atteindre la tête du chenal (Bugden, 1991 ; Drinkwater et Gilbert, 2004 ; Gilbert et al., 2005 ; Stevens et al., 2024). Deux phénomènes sont responsables du développement des conditions hypoxiques que l'on retrouve depuis environ 1985 dans les eaux profondes de l'estuaire maritime et, maintenant, dans la partie ouest du golfe du Saint-Laurent : un changement de la contribution relative des eaux parentales (courant labrador et Gulf Stream) aux eaux profondes et une augmentation des taux de reminéralisation aérobique de la matière organique qui est livrée à celles-ci (Gilbert et al., 2005 ; Thibodeau et al., 2006 ; Jutras et al., 2020, 2023a, 2023b).

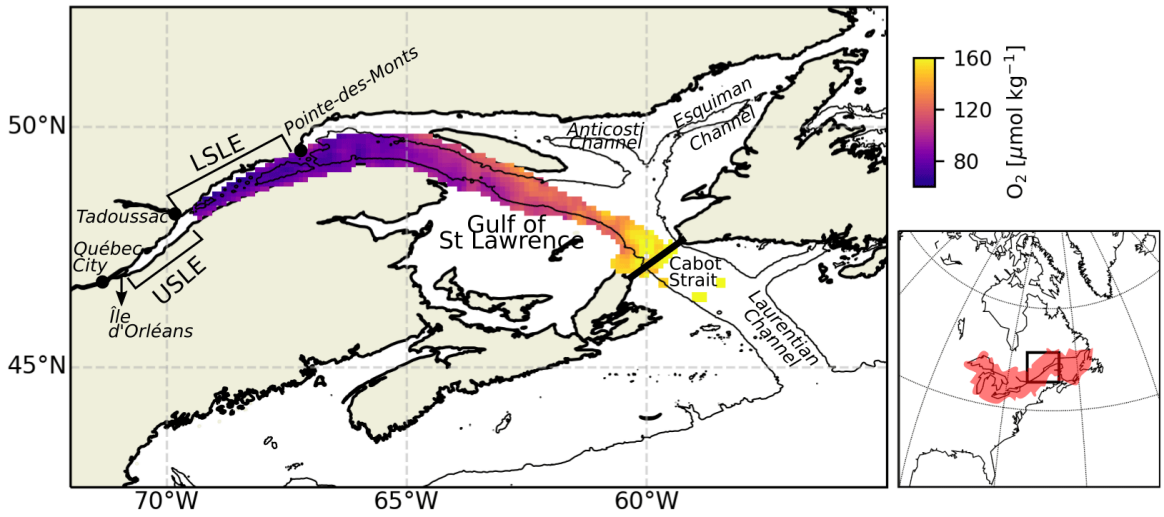

Figure 3. Carte de l'estuaire maritime du Saint-Laurent avec les concentrations minimales en oxygène dissous entre 1970 et 2018. L'estuaire maritime du Saint-Laurent est désigné par l'acronyme LSLE pour Lower St. Lawrence Estuary. La carte de droite montre le bassin versant du système Saint-Laurent (tiré de Jutras et al. 2023a)

Compte tenu de la forte stratification qui caractérise l'estuaire maritime du Saint-Laurent, les eaux profondes sont isolées des eaux de surface et ne sont réoxygénées que par diffusion et turbulence à proximité de la tête du chenal. Par conséquent, les concentrations en oxygène dissous dans celles-ci diminuent progressivement à mesure qu'elles transitent vers l'amont alors que la reminéralisation microbienne aérobique de la matière organique, qui sédimente à travers la colonne d'eau, consomme l'oxygène. Cela mène au développement d'une hypoxie qui s'est intensifiée au cours du dernier siècle et qui de s'intensifier encore au cours des prochaines années (Jutras et al., 2023a, 2020; Gilbert et al., 2005). La superficie de la zone dite hypoxique est déjà passée de ~1300 km^2 en 1993 à ~9400 km^2 en 2021 (Jutras et al., 2023a).

Le développement de l'hypoxie dans le chenal laurentien affecte les processus de minéralisation de la matière organique enfouie en réduisant la profondeur de pénétration de l'oxygène dans les sédiments, entraînant une augmentation de la respiration anaérobie de la dégradation de la matière organique, ce qui mène à la fois à une augmentation des taux de sulfato-réduction (Katsev et al., 2007) et à une limitation de la disponibilité des oxydants nécessaires à la réoxydation des espèces soufrées réduites comme le $\sum H_2S$. De plus, une décroissance de l'abondance et de la diversité d'espèces benthiques et épibenthiques en conditions hypoxiques limite la bioturbation et la bio-rrigation des sédiments, ce qui réduit davantage la profondeur de la couche de mélange et la pénétration d'espèces oxydantes dans les sédiments (Pascal et al., 2024).

Minéralisation de la matière organique : séquence des réactions cataboliques durant la diagenèse précoce dans les sédiments marins

La production de $\sum H_2S$ dans les sédiments marins s'inscrit dans une séquence de réactions microbienne de dégradation de la matière organique désignée par le terme de diagenèse précoce. Ce terme englobe l'ensemble des processus physiques, chimiques et biologiques post-dépositionnels qui se produisent dans les sédiments aquatiques. La majorité

de ces processus sont directement ou indirectement liés à la dégradation microbienne de la matière organique (Froelich et al., 1979). La reminéralisation de la matière organique dans les sédiments marins se fait selon une séquence de réactions cataboliques dictée, selon la disponibilité et la nature des oxydants, par l'énergie libre de la réaction d'oxydation (Froelich et al., 1979 ; Jørgensen, 2006; Sundby, 2006) (Tableau 1).

Tableau 1. Séquence des réactions simplifiées d'oxydation de la matière organique avec leur énergie libre standard, ΔG^0, par mole de carbone organique. CH_2O représente la matière organique de composition non-spécifiée. Les valeurs de ΔG^0 sont données à pH 7, issu de Jørgensen (2006)

	Réaction et stœchiométrie	ΔG^0 (kJ mol^{-1})	
Zone oxique	Respiration aérobique $CH_2O + O_2 \rightarrow CO_2 + H_2O$	-479	(1)
Zone anoxique	Dénitrification $5(CH_2O) + 4\ NO_3^- \rightarrow 2\ N_2 + 4\ HCO_3^- + CO_2 + 3\ H_2O$	-453	(2)
	Réduction des oxydes de manganèse $CH_2O + 3\ CO_2 + H_2O + 2\ MnO_2 \rightarrow 2\ Mn^{2+} + 4\ HCO_3^-$	-349	(3)
	Réduction des oxydes de fer $CH_2O + 7\ CO_2 + 4\ Fe(OH)_3 \rightarrow 4\ Fe^{2+} + 8\ HCO_3^- + 3\ H_2O$	-114	(4)
	Réduction des sulfates $2(CH_2O) + SO_4^{2-} \rightarrow H_2S + 2\ HCO_3^-$	-77	(5)
	Méthanogenèse $4\ H_2 + HCO_3^- + H^+ \rightarrow CH_4 + 3H_2O$	-136	(6)

La première réaction catabolique lors de la reminéralisation de la matière organique est la respiration aérobie, qui est aussi la principale voie de dégradation de matière organique dans une colonne d'eau oxygénée. Dans les sédiments, l'oxygène dissous est rapidement consommé par les micro-organismes pour transformer la matière organique en dioxyde de carbone selon l'équation (1) du Tableau 1.

Lorsque l'oxygène est épuisé dans les eaux porales du sédiment, ce dernier devient anoxique. Les micro-organismes utilisent alors des accepteurs d'électrons alternatifs pour la minéralisation de la matière organique sous des conditions anaérobiques, selon un ordre dicté par l'énergie libre de la réaction de potentiel d'oxydoréduction décroissant. Ainsi, les nitrates (eq. 2), les oxydes de manganèse (eq. 3), les oxydes de fer (eq. 4), et enfin les sulfates (eq. 5) sont utilisés successivement (Froelich et al., 1979) (Tableau 1). Les composés réduits issus de ces réactions et dissous dans les eaux porales migrent vers la zone oxique, suivant leur gradient de concentration. Dans la zone oxique, ils peuvent être réoxydés par l'oxygène ou d'autres oxydants comme les nitrates et les oxydes métalliques (Fig. 2).

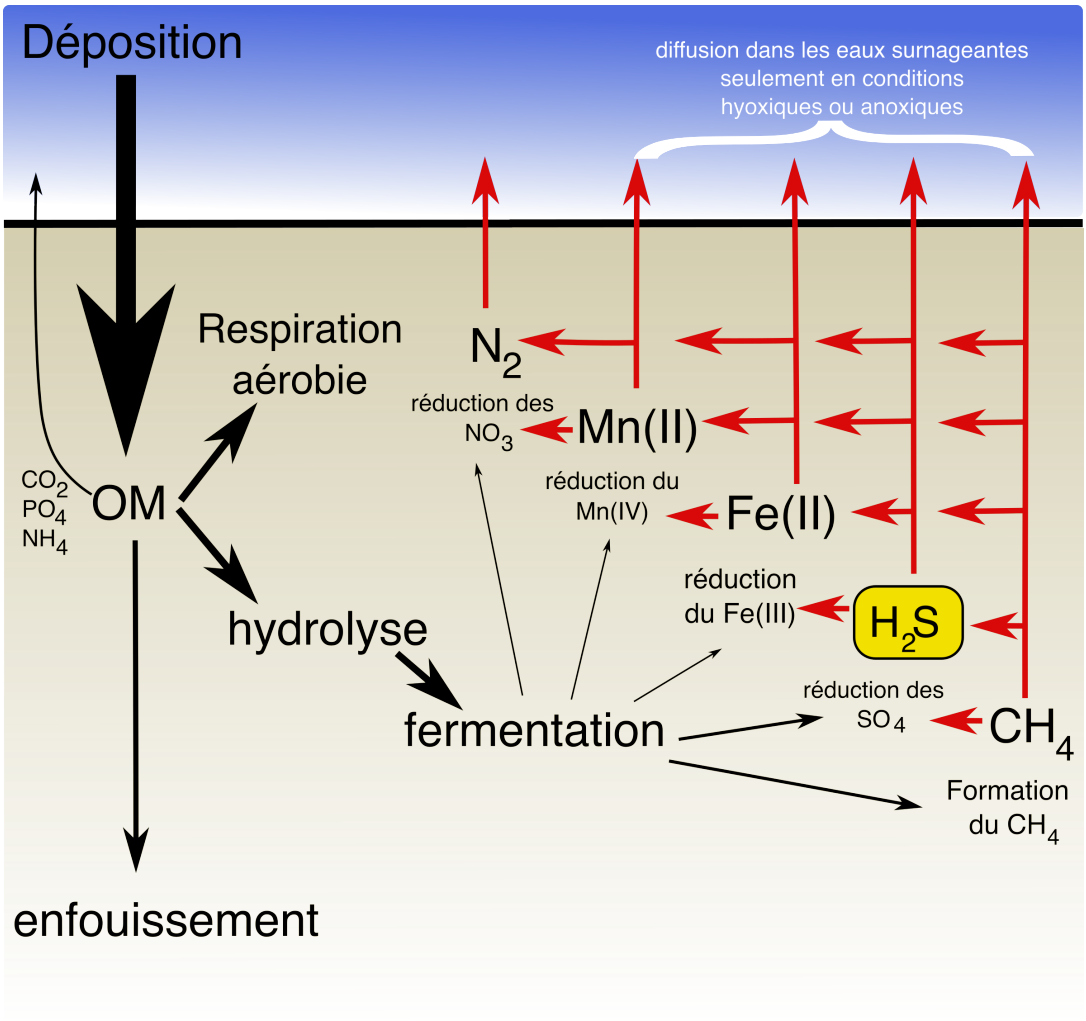

Figure 4. Modèle conceptuel de la dégradation de la matière organique (OM) et des voies de ré-oxidation (basé sur Jørgensen, 2006 ; Middelburg et Levin, 2009 ; Middelburg, 2019) Les flèches rouges représentent le devenir des produits réduits libérés et dissous pendant la minéralisation anaérobique.

La diminution de la concentration d'oxygène dans la colonne d'eau affecte cette séquence, la compressant près de l'interface eau-sédiment, laissant une place prépondérante à la dégradation anaérobie au détriment de la dégradation aérobie, ce qui consomme plus rapidement les accepteurs d'électrons alternatifs. Cependant, il a été démontré que

l'abondance en oxydes métalliques peut avoir un effet tampon sur l'impact de la désoxygénation des eaux profondes sur la diagenèse précoce ; une forte abondance d'oxydes métalliques permettrait de retarder l'altération de la séquence redox (Soetaert et al., 2000 ; Middelburg et Levin, 2009).

Cycle du soufre, production et devenir du $\sum H_2S$

Puisque l'océan représente l'un des plus grands réservoirs de sulfates sur terre, la sulfato-réduction contribue à une grande partie de la reminéralisation de la matière organique en milieu côtier (Vairavamurthy et al. 1995; Jørgensen, 1982). Les variations dans la séquence des réactions cataboliques durant la diagenèse précoce influencent non seulement la production de $\sum H_2S$ mais aussi leur devenir. La désoxygénation de la colonne d'eau, la vitesse de sédimentation et la disponibilité de fer réactif peuvent affecter le devenir du $\sum H_2S$ dont sa précipitation, son enfouissement et sa ré-oxydation dans les sédiments.

Le cycle du soufre repose sur des interactions complexes entre plusieurs espèces chimiques, notamment les sulfates (SO_4^{2-}), les sulfures ($\sum H_2S$, AVS, pyrite) et les composés d'état d'oxydation intermédiaires (ex. soufre élémentaire, polysulfures). Une partie du soufre peut aussi être incorporée dans la matière organique, il s'agit du soufre organique (Gagnon, 1996 ; Canfield et al., 1998). La répartition de ces espèces chimiques est étroitement liée à la dégradation de la matière organique et aux conditions redox dans les sédiments (Jørgensen, 1982). La sulfato-réduction microbienne dissimilatrice (eq. 5) produit du $\sum H_2S$. Ce $\sum H_2S$ peut ensuite être précipité avec le fer réactif présent dans les sédiments pour former des sulfures acides volatiles (AVS) métastables, principalement FeS (Eq. 7) ou être réoxydé sous formes de sulfates (Eq.8) ou d'espèces soufrées au degré d'oxydation intermédiaire comme le soufre élémentaire (S(0) ; Eq. 9) et les polysulfures (S_n(-II)) ; Chen et Gupta, 1973; Boulegue, 1976; Steudel, 2003; Kamyshny et al., 2004, 2014; Kafantaris et Druschel, 2020).

$HS^- + Fe^{2+} \rightarrow FeS + H^+$ (7)

$HS^- + 2O_2 \rightarrow SO_4^{2-} + H^+$ (8)

$2HS^- + O_2 \rightarrow 1/4\ S_8 + 2OH^-$ (9)

La formation des AVS constitue une étape transitoire entre la production de $\sum H_2S$ et la précipitation de pyrite (FeS_2), le principal puit de soufre et de fer en milieu marin (Berner, 1978, 1984 ; Berner et al., 1997 ; Rickard and Luther, 2007).

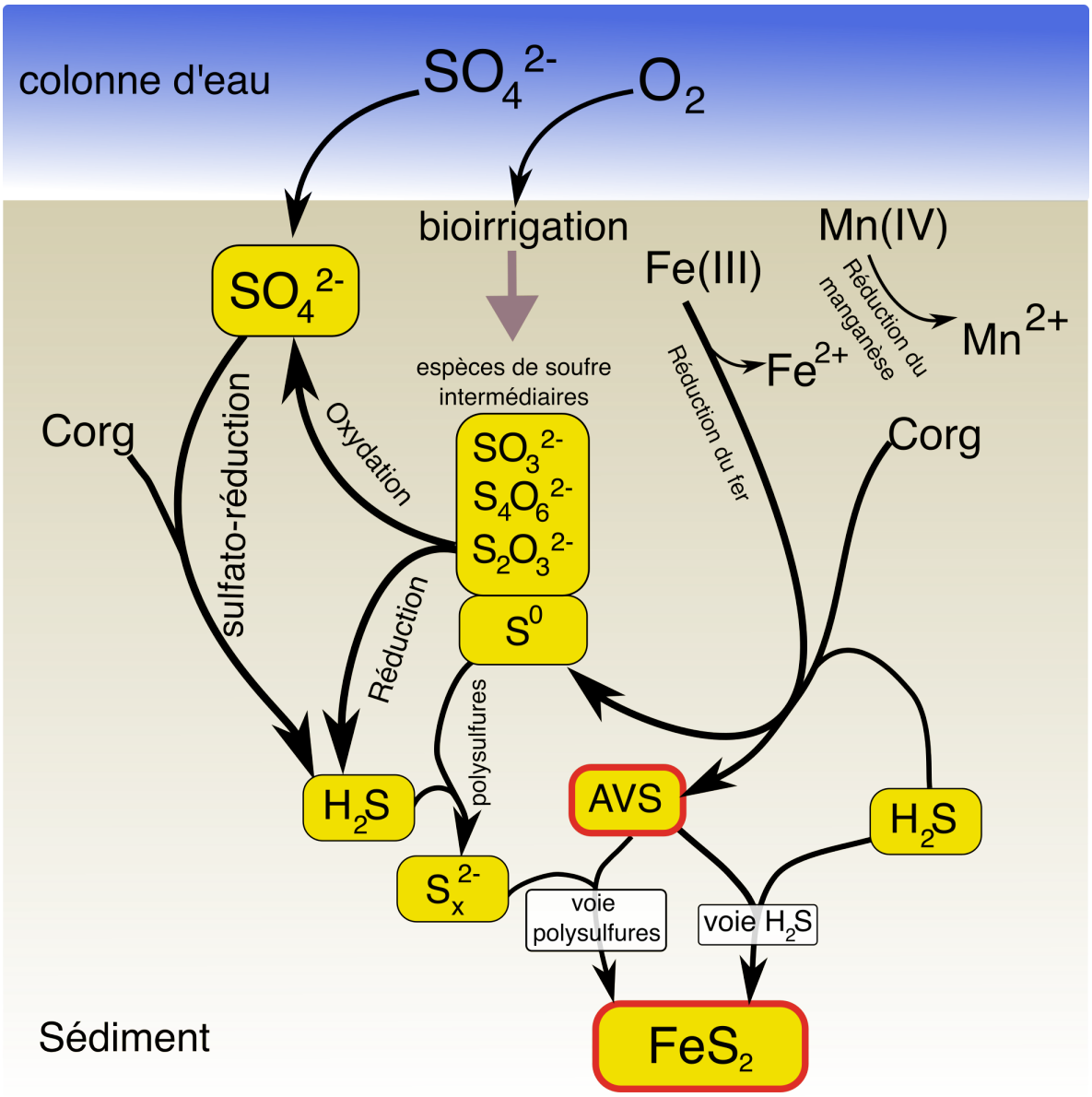

Figure 5. Le cycle biogéochimique du soufre dans les sédiments marins. La représentation schématique est simplifiée et modifiée de Jørgensen et al. (2019). Les flèches indiquent les flux et les voies réactionnelles microbiennes et chimiques. Les encadrés rouges identifient les espèces particulaires soufrées dont la distribution est étudiée dans la présente étude

La transformation des AVS métastables en pyrite s'effectue selon deux voies réactionnelles. La première est la « voie H_2S » (Eq. 10) (Rickard, 1975; Luther, 1991) où les

monosulfures de fer réagissent avec le sulfure dissous, cette voie réactionnelle requiert une concentration élevée de $\sum H_2S$ dans les sédiments.

$$FeS + H_2S \rightarrow FeS_2 + H_2 \qquad (10)$$

La seconde est appelée « voie polysulfures » (Eq.11) (Rickard, 1975; Luther, 1991), où les monosulfures de fer réagissent avec les polysulfures. Les polysulfures proviennent de la réaction entre le sulfure dissous et le soufre élémentaire, la réaction nette de la formation de la pyrite par cette voie réactionnelle est l'addition apparente du soufre élémentaire au monosulfure de fer (Butler et al., 2004) :

$$FeS + S^0 \rightarrow FeS_2 \qquad (11)$$

Ainsi, la transformation des AVS en pyrite nécessite soit une concentration élevée de H_2S, soit la présence d'oxydants permettant la formation de polysulfures. Dans les deux cas, la concentration en oxygène dans les eaux profondes ainsi que la disponibilité de fer réactif dans les sédiments influencent la distribution des AVS et de la pyrite.

Disponibilité du fer réactif

La formation d'AVS et de pyrite est en partie contrôlée par la disponibilité du soufre et celle du fer réactif (Berner, 1984; Rickard et Luther 2007; Liu et al. 2021). Les sédiments du chenal laurentien sont particulièrement riches en fer compte tenu de l'apport de sédiments du bouclier canadien contenant notamment des roches grenvilliennes riches en feldspaths potassique, amphiboles, plagioclase et magnétite (Loring et Nota, 1968, 1973; Gagnon et al.,

1995; Gobeil, 2006; Jaegle, 2015). Les interactions entre le cycle du fer et celui du soufre interviennent à plusieurs étapes de la minéralisation de la matière organique. Premièrement, le Fe(III) est l'accepteur d'électron qui précède les sulfates dans la séquence redox de reminéralisation de la matière organique sédimentaire (Eq. 4). Le produit réduit de la réduction des oxydes de Fe(III) est le Fe(II), qui réagit ensuite avec le $\sum H_2S$ pour produire des AVS (Eq. 7). Cependant, dans la zone de production des AVS, des radicaux libres de sulfure peuvent aussi réagir avec le Fe(III) pour former du soufre élémentaire, le Fe(II) produit réagit ensuite avec le $\sum H_2S$ pour former des AVS.

Les (hydr)oxydes de fer sont plus ou moins réactifs, les espèces amorphes et peu crystallines comme la ferrihydrite et la lepidocrocite réagissent rapidement avec le sulfure d'hydrogène (leur demi-vie se compte en heures ou en jours). Les oxides plus cristallins comme la goethite et l'hématite réagissent un peu plus lentement (demi-vie d'environ un mois) tandis que la réactivité de la magnétite est plus variable, allant de quelques mois à une centaine d'années (Canfield et al., 1992, Raiswell et al., 1994; Poulton et Raiswell, 2005; Poulton et Canfield, 2005; Zhu et al. 2012).

Une augmentation du réservoir de fer réactif sédimentaire a été observé à la tête du chenal laurentien après 25 ans d'hypoxie persistante (Lefort et al., 2012). Cette augmentation pourrait être le résultat d'une longue exposition de minéraux silicatés moins réactifs aux sulfures, entraînant leur dissolution et l'augmentation de leur réactivité (Canfield et al., 1992; Lefort et al., 2012). Cette interprétation repose sur un bilan de masse du fer total et sa redistribution parmi les phases réactives, incluant le dissous ainsi que sur l'hypothèse d'une augmentation des taux de sulfato-réduction et de la production de $\sum H_2S$ au fur et à mesure du développement et de l'aggravation de l'hypoxie dans le chenal laurentien (Kastev et al., 2007). De plus, il a été suggéré que cet enrichissement en fer réactif favorise la précipitation d'AVS, limite l'accumulation de $\sum H_2S$ et sa diffusion dans les eaux porales et, par conséquent, inhibe la conversion des AVS en pyrite (Lefort et al., 2012).

Lorsque le fer réactif est abondant dans les sédiments, comme c'est le cas dans le chenal laurentien, le $\sum H_2S$ produit est rapidement précipité sous forme d'AVS et la voie « H_2S » de

conversion des AVS en pyrite n'est pas efficace (Gagnon et al., 1995, 1996). La voie réactionnelle privilégiée dans ce cas est donc la « voie polysulfures » (Gagnon et al., 1995, 1996). La conversion des AVS en pyrite dans un milieu riche en fer repose alors principalement sur la disponibilité d'oxydants qui permettent la réoxydation du $\sum H_2S$ et la production de polysulfures. Plusieurs facteurs environnementaux peuvent influencer la disponibilité en oxydants, incluant les concentrations en oxygène dissous des eaux profondes, les taux de sédimentation et d'accumulation de carbone organique, ainsi que l'activité des organismes benthiques et épibenthiques (bioturbation et bio-irrigation) (Rickard et Morse, 2005).

Le chenal Laurentien, un milieu riche en fer et soumis à une désoxygénation persistante, offre un terrain d'étude unique pour comprendre l'impact de l'hypoxie sur le cycle du soufre et son interaction avec le cycle du fer. L'abondance de fer réactif dans les sédiments limite l'accumulation du $\sum H_2S$ dans les eaux porales, promeut sa précipitation sous forme d'AVS et inhibe la formation de pyrite. Il demeure important d'évaluer la capacité tampon de cette abondance en fer réactif, car elle peut être un indicateur du potentiel de résilience de l'écosystème face au changement environnemental rapide que constitue la désoxygénation.

Objectifs et hypothèses de travail

Il a été proposé que la diminution de la concentration en oxygène dissous dans les eaux profondes de l'estuaire maritime du Saint-Laurent mène à une augmentation de la proportion de matière organique sédimentaire qui est minéralisée par la sulfato-réduction et donc à une augmentation de la production de $\sum H_2S$ (Katsev et al., 2007). Il a aussi été suggéré que la désoxygénation persistante pourrait entraîner une augmentation de la formation d'AVS et interférer avec la production de pyrite (Lefort et al, 2012). Cependant, ces hypothèses doivent être confrontées à la réalité d'environnements sédimentaires complexes, où de nombreux

facteurs influencent simultanément la répartition des espèces soufrées. Parmi ces facteurs, la quantité et la réactivité de la matière organique, la disponibilité en fer réactif, les taux de sédimentation et la réoxydation des espèces réduites jouent un rôle déterminant. Il s'agit donc d'élucider la contribution relative de ces paramètres environnementaux pour expliquer les variations de la distribution des espèces soufrées à différentes stations du chenal laurentien. **L'objectif général de cette étude est donc de comprendre le devenir des sulfures d'hydrogène ($\sum H_2S$) dans les sédiments du chenal laurentien en contexte d'hypoxie persistante.** Pour répondre à cette problématique, trois objectifs spécifiques ont été définis :

1) Quantifier et analyser la répartition verticale et spatiale des principales espèces soufrées dans les sédiments (AVS et pyrite).

2) Étudier l'impact de facteurs environnementaux sur la répartition des espèces soufrées : la quantité (C_{org}) et de la réactivité ($\delta\ ^{13}C$) de la matière organique sédimentaire, la disponibilité du fer réactif solide et les taux de sédimentation.

3) Évaluer la capacité tampon des sédiments du LSLE à limiter l'accumulation $\sum H_2S$ dans les eaux porales selon la disponibilité du fer minéral réactif.

Ces objectifs visent à identifier les mécanismes qui contrôlent la dynamique des espèces soufrées en condition d'hypoxie persistante et à mieux comprendre la résilience biogéochimique des sédiments du chenal laurentien face aux changements environnementaux.

Contribution de l'auteure

Le chapitre de ce mémoire est présenté sous forme d'article scientifique rédigé en anglais et intitulé « Deoxygenation and the buffering effect of reactive iron on the distribution of sulfur species in the St. Lawrence Estuary sediments». Les premiers résultats ont été présentés dans des congrès nationaux (réunion scientifique annuelle de Québec Océan, 2023 et au congrès des étudiant.e.s du GEOTOP, 2023).

Toutes les données présentées dans le cadre de ce mémoire sont issues de deux missions d'échantillonnage ayant eu lieu en 2022 (16 mai au 22 mai) et 2023 (22 mai au 26 mai) à bord du N/R Coriolis II. J'ai participé aux deux missions. J'ai extrait les AVS et la pyrite des sédiments après avoir adapté les méthodes conventionnelles aux laboratoires de l'UQAR-ISMER. J'ai préparé les échantillons pour les analyses élémentaires de carbone qui ont été effectuées au Laboratoire de géochimie des isotopes stables légers à l'Université du Québec à Montréal (GEOTOP-UQÀM, Montréal, QC, Canada). Santiago Marques et Camille Tran, lors de leur stage en 2023, ont effectué les mesures de fer réactif. Santiago Marques a aussi effectué les mesures de sulfates dissous. Camille Tran et moi-même avons effectué les mesures de porosité du sédiment. Les mesures d'oxygène dissous ont été effectuées par Ludovic Pascal et Arturo Zanon lors de la mission de 2023. J'ai effectué les analyses granulométriques dans le laboratoire de Jean-Carlos Montero-Serrano à L'UQÀR-ISMER. Les résultats des analyses granulométriques ont été traitées statistiquement à l'aide du programme GRADISTAT. J'ai produit toutes les figures présentées dans ce mémoire sauf les figures 1 et 3.

CHAPITRE 1
DÉSOXYGÉNATION ET EFFET TAMPON DU FER RÉACTIF SUR LA RÉPARTITION DES ESPÈCES SOUFRÉES DANS LES SÉDIMENTS DE L'ESTUAIRE MARITIME DU SAINT-LAURENT

1.1 RÉSUMÉ EN FRANÇAIS DE L'ARTICLE

Le développement de zones hypoxiques dans les eaux continentales et côtières est une préoccupation croissante à l'échelle mondiale. La désoxygénation, c'est-à-dire la diminution des concentrations en oxygène dissous dans les systèmes aquatiques, jusqu'à atteindre des niveaux hypoxiques (< 63 μmol/L), a fait l'objet de nombreuses études au cours des dernières décennies. Certaines facettes de ses effets sur les différents milieux estuariens et côtiers sont encore mal connues. Ce phénomène peut avoir des répercussions importantes sur la santé des écosystèmes aquatiques, notamment le déclin de l'abondance et de la diversité d'espèces pélagiques et benthiques, l'activité (bioturbation, bio-irrigation) de ces dernières, ainsi que la perturbation des principaux cycles biogéochimiques. L'appauvrissement en oxygène dissous des eaux profondes limite la minéralisation aérobique, favorisant ainsi la respiration anaérobique de la matière organique sédimentaire tout en diminuant le potentiel de réoxydation des espèces réduites. Dans l'estuaire maritime du Saint-Laurent (LSLE pour Lower St. Lawrence Estuary), la désoxygénation des eaux profondes depuis au moins les années 1930 a entraîné une augmentation de la sulfato-réduction et de la production de sulfure d'hydrogène ($\sum H_2S = H_2S + H_S^-$). Dans les sédiments riches en fer, tels que ceux de l'estuaire maritime du Saint-Laurent, le $\sum H_2S$ est précipité sous forme de sulfures acides volatiles (AVS) métastables, limitant son accumulation dans les eaux porales. La conversion ultérieure de ces AVS métastables en pyrite (FeS_2), qui est le principal puit de soufre dans les milieux marins, dépend de plusieurs paramètres environnementaux dont la concentration en $\sum H_2S$ dans les eaux porales, l'abondance de fer réactif ainsi que la disponibilité

d'oxydants dans les sédiments. En revanche, dans les systèmes limités en fer, la désoxygénation peut entraîner une accumulation de $\sum H_2S$ dans les eaux porales et son éventuelle diffusion dans les eaux surnageantes. Cette étude vise à comprendre le devenir du sulfure d'hydrogène dans les sédiments du LSLE dans le contexte d'une hypoxie persistante. Les principaux objectifs visent à 1) établir un portait du cycle du soufre dans les sédiments actuels du LSLE, 2) identifier les paramètres environnementaux qui influencent ce cycle, 3) évaluer la disponibilité du fer réactif et son interaction avec le cycle du soufre. Basés sur trois sites distincts du LSLE, nos résultats suggèrent que les taux de sédimentation jouent un rôle plus déterminant que la concentration en oxygène dissous de la colonne d'eau sur la répartition des espèces soufrées. Bien que les taux d'accumulation et l'origine de la matière organique sédimentaire diffèrent sensiblement entre les sites à l'étude, le taux d'accumulation des espèces soufrées (AVS + pyrite) est semblable, mais l'abondance relative des AVS métastables et de la pyrite, plus stable, varie significativement. Le ratio AVS-S :Pyrite-S atteint 0.9 aux sites ayant le plus rapide taux de sédimentation (0.4 ± 0.03 cm yr^{-1} et 0.3 ± 0.03 cm yr^{-1}), contre moins de 0.2 au site ayant un taux de sédimentation plus lent (0.2 ± 0.03 cm yr^{-1}). Ces différences expliqueraient une conversion plus efficace des AVS en pyrite au site ayant le taux de sédimentation le plus lent et donc une variabilité dans la stabilité du puit de soufre. L'abondance de fer réactif (> 200 µmol/g) à tous les sites ne semble pas être un facteur limitant pour la précipitation des $\sum H_2S$. Nos observations suggèrent que les variations, même légères, des taux de sédimentation, en isolant plus ou moins rapidement les AVS de l'interface eau-sédiment (SWI), limite l'accès aux oxydants nécessaires à la formation d'espèces soufrées d'états d'oxydation intermédiaire et la transformation des AVS en pyrite. Bien que la répartition des espèces soufrées dans les sédiments soit variable, l'abondance de fer réactif est un tampon efficace contre l'accumulation de $\sum H_2S$ dans les eaux interstitielles du LSLE et prévient l'éventuelle diffusion de ces espèces toxiques dans la colonne d'eau.

1.2 DEOXYGENATION AND THE BUFFERING EFFECT OF REACTIVE IRON ON THE DISTRIBUTION OF SULFUR SPECIES IN THE LOWER ST. LAWRENCE ESTUARY SEDIMENTS

Gwenn Duval[1], Alfonso Mucci[2], Gwénaëlle Chaillou[1], André Pellerin[1]

[1] Québec-Océan et Institut des Sciences de la Mer, Université du Québec à Rimouski, 310 Allée des Ursulines, Rimouski, Québec, Canada, G5L 2Z9.

[2] GEOTOP and Department of Earth and Planetary Sciences, McGill University, 3450 University Street, Montréal, Québec, Canada, H3A 0E8.

1.3 INTRODUCTION

The global increase in documented hypoxic zones in coastal waters is a growing concern due to their impact on marine ecosystems and the organisms inhabiting these environments (Diaz and Rosenberg, 2008; Rabalais et al., 2009; Breitburg et al., 2018). Deoxygenation – defined as the decline in dissolved oxygen concentrations ([DO]) in aquatic systems may eventually lead to hypoxia when [DO] fall below 63 µmol/L (Diaz and Rosenberg, 1995; Keeling et al., 2010; Falkowski et al., 2011; Fredriksson et al., 2024). Hypoxia can have deleterious impacts on marine ecosystems, including decreasing the abundance and diversity of pelagic and benthic organisms, the activity (bioturbation, bio-irrigation) of the latter as well as the disruption of key biogeochemical cycles (Middelburg and Levin, 2009; Sturdivant et al., 2012; Beam et al., 2022; Pascal et al., 2024).

Bottom-water deoxygenation occurs under strong water column stratification, when water masses are isolated from exchange with oxygen-rich surface waters and cannot readily be replenished in oxygen (Diaz, 2001; Gilbert et al., 2005; Zhang et al., 2010). The consumption of dissolved oxygen for the respiration and aerobic mineralization of organic matter in these bottom waters and the underlying sediment, therefore, depletes the [DO] pool, ultimately leading to anoxia or even euxinia when $[DO]_{bot}$ (bottom-waters dissolved oxygen

concentrations) become null (Diaz, 2001; Rabalais et al., 2009). The development of bottom-water hypoxia or anoxia can be a seasonal phenomenon in regions like the Gulf of Mexico, Aarhus Bay (Denmark), and Long Island Sound (New York, USA) (Diaz, 2001; Conley et al., 2007; Whitney and Vlahos, 2021, Rabouille et al., 2021) or be more persistent and last the whole year in locations such as the St. Lawrence Estuary, the Caspian Sea or the Gulf of Finland (Peeters et al., 2000; Diaz, 2001; Jutras et al., 2023a; Stoicescu et al., 2024). Seasonal bottom-water hypoxia is followed by periods of weak stratification or destratification, typically in response to cooling of surface waters and mixing of the water column and a large input of oxygen to depth seasonally, that usually occurs during fall and winter (Conley et al., 2007; Zhang et al., 2010). On the other hand, persistent hypoxia is associated with a constant and strong stratification of the water column and, therefore, continuous physical isolation of the bottom-waters from more oxygenated waters and the atmosphere, leading to a progressive decline with time in $[DO]_{bot}$ (Stoicescu et al., 2024; Rabalais et al., 2009). Hence, the biogeochemical response of sediments to deoxygenation varies significantly depending on whether hypoxia is persistent or seasonal (Diaz, 2001; Zhang et al., 2010; Kennet and Ingram, 1995; Gooday et al., 2009, Rabouille et al., 2021).

The $[DO]_{bot}$ impact the pathways of organic matter (OM) mineralization. Oxygen depletion reduces the efficiency of aerobic mineralization, shifting the balance toward anaerobic pathways (Berner, 1980; Soetaert et al., 2000; Burdige, 2006; Middelburg and Lavin, 2009). Once oxygen is exhausted in the sediments, anaerobic respiration proceeds according to a sequence dictated by the free energy yield of the catabolic reactions with different electron acceptors, starting with nitrate, manganese oxides, iron oxides, and sulfate (Burdige, 2006; Froelich et al., 1979). In the presence of well-oxygenated overlying waters, reduced species produced by anaerobic respiration in the sediment can be re-oxidized if they are introduced by diffusion or mechanical mixing into the oxic zone (Jørgensen, 1982; Middelburg and Levin, 2009). Bottom-water deoxygenation will compress the sequence of catabolic reactions towards the sediment-water interface, promote the anaerobic remineralization of OM, and render the re-oxidation of reduced compounds less effective (Jessen et al., 2017; Kastev et al., 2007; Middelburg and Levin, 2009). Coastal sediments

rich in iron and manganese oxides can, however, buffer against these effects of deoxygenation, delaying shifts in redox processes compared to sediments poor in oxidants other than sulfate (Middelburg and Levin, 2009; Soetaert et al., 2000).

Sulfate-reducing bacteria in sediments oxidize OM to HCO_3^- while reducing sulfate in porewater to H_2S and HS^- ($\sum H_2S$). The fate of $\sum H_2S$, produced by sulfate-reduction (SR), is complex as it can either be re-oxidized in the sediments by available oxidants (oxygen, nitrates, and manganese oxides) (Aller and Rude, 1988; Schippers and Jørgensen, 2002) or react with reduced dissolved iron, Fe(II), to form acid volatile sulfides (AVS), mainly FeS, before its conversion into more stable pyrite (Rickard et al., 1999). The term "AVS" refers to a complex and variable component, including solid phases (Mackinawite (FeS) and Greigite (Fe_3S_4) but also dissolved iron-sulfur clusters and nanoparticles (Rickard and Morse, 2005). AVS is an operationally defined component that produces H_2S when HCl is added to the sediment (Berner, 1964; Rickard and Morse, 2005). In this article, the term "pyrite" will be used to refer to the operationally defined chromium-reducible sulfur (CRS) fraction that primarily includes pyrite (FeS_2) (Cornwell and Morse, 1987). The conversion from AVS to pyrite involves two main pathways: the "H_2S" pathway (Eq. 1), requiring high porewater $\sum H_2S$ concentrations, and the "polysulfide pathway" (Eq. 2) that involves intermediate sulfur species like elemental sulfur (S(0)) and polysulfides (general formula of $S_n(-II)$, with n ranging from 2 to 8 in natural systems) that form during the partial oxidation of $\sum H_2S$ (Chen and Gupta, 1973; Boulegue, 1976; Steudel, 2003; Kamyshny et al., 2004, 2014; Kafantaris and Druschel, 2020).

$$FeS + H_2S \rightarrow FeS_2 + H_2 \qquad (1)$$

$$FeS + S^0 \rightarrow FeS_2 \qquad (2)$$

The net reaction of the polysulfide pathway is the apparent addition of zero-valent S from $S_n(-II)$ to FeS (Butler et al., 2004).

The dominance of one pathway over the other is influenced by oxygen availability, sedimentation rates, and the availability of reactive iron (Rickard and Morse, 2005). The

designated reactive iron pool encompasses the dithionite-soluble (oxyhydr)oxides such as ferrihydrite, lepidocrocite, goethite and hematite, in addition to the iron that was transformed to pyrite, according to the definition of highly reactive iron of Poulton and Canfield (2005). Under oxygen-depleted bottom-water conditions, the increased reliance on anaerobic catabolic processes results in higher porewater $\sum H_2S$ concentrations with limited re-oxidation potential (Katsev et al., 2007; Howart et al., 2011; Park et al., 2020). The distribution of sulfur and reactive iron species has been used as an indicator of the health of ecosystems as well as to identify past and present euxinic conditions (Cornwell and Morse, 1987; Thode-Andersen and Jørgensen, 1989; Fossing and Jørgensen, 1990; Middleburg, 1991; Gagnon et al., 1995, Raiswell and Canfield, 2012). Euxinic environments are characterized by anoxic bottom-waters and the presence of $\sum H_2S$ in the water column. When the production of $\sum H_2S$ exceeds the availability of reactive iron and other oxidants, including oxygen in the overlying waters, porewater $\sum H_2S$ may diffuse and accumulate in the bottom-waters, leading to euxinia and fish death by toxicity (Luther et al., 2004). Hydrogen sulfide exposure has also been shown to accelerate hypoxia-driven mortality of benthic macrofauna (Vaquer-Sunyer and Duarte, 2010), underlying the importance of studying the indirect effects of hypoxia development in coastal areas.

The activity of benthic organisms also plays a crucial role in sedimentary sulfur cycling by enhancing the re-oxidation of AVS and $\sum H_2S$ (Rickard and Morse, 2005). Bio-irrigation introduces oxygen and other oxidants deeper into the sediment (Aller, 1977; Kristensen et al., 2002) whereas bioturbation brings up solid reduced compounds such as AVS to the oxic layer. Under hypoxic conditions, reduced benthic and epibenthic activity may limit re-oxidation processes (Pascal et al., 2024), affecting the distribution of sulfur species and contributing to the accumulation of reduced compounds in the sediment (Beam et al., 2022; Rickard and Morse, 2005).

The impacts of deoxygenation on the sulfur species distribution in sediments depend on several factors. In iron-poor systems, hypoxia can lead to the buildup of porewater $\sum H_2S$, whereas iron-rich sediments may buffer against this accumulation by precipitation of AVS.

The subsequent conversion of AVS to pyrite seems to be controlled both by the availability of reactive iron and oxidants (Aller, 1977; Thode-Anderson and Jørgensen, 1989; Oenema, 1990; Middelburg, 1991; Gagnon et al., 1995; Schippers and Jørgensen, 2002; Goldhaber and Kaplan, 1974; Rickard and Morse, 2005). Rapid pyrite formation near the sediment-water interface (SWI) has been observed in some sulfidic systems, where the H_2S pathway dominates (Liu et al., 2021). On the other hand, the accumulation of AVS have been observed in high sedimentation rate environments, where the distance between the locus of AVS formation and oxidant availability can limit re-oxidation (Gagnon et al., 1995; Rickard and Morse, 2005). In other words, the response of the biogeochemical sulfur cycle to bottom-water deoxygenation is highly dependent on specific local conditions; hence, the study of the LSLE sediments allows us to better identify some of the factors that control the burial of sulfur species under hypoxic conditions.

Katsev et al. (2007) predicted that persistent bottom-water deoxygenation in the Lower St. Lawrence Estuary (LSLE) would increase sulfate reduction rates (SRR) and $\sum H_2S$ production, potentially altering the sulfur cycle in these sediments. The sediments of the LSLE are iron-rich (Casse et al., 2017; Gagnon et al., 1995, 1996). Hence, we expect the reactive iron to buffer the accumulation of porewater $\sum H_2S$ by precipitating it as iron sulfides. After three decades of worsening hypoxia in the LSLE (Jutras et al., 2023a, 2020; Gilbert et al., 2005), this study is an opportunity to evaluate the evolution of this buffering capacity.

The primary objective of this study was to understand the fate of porewater $\sum H_2S$ in the iron-rich sediments of the LSLE under persistent bottom-water hypoxia. To do so, we 1) analyzed the spatial and vertical distribution of AVS and pyrite, the two principal sulfur sinks in the sediments, 2) investigated the impact of environmental factors on ttheir distribution in the specific context of the LSLE, including organic matter quantity and reactivity, reactive iron availability, and sedimentation rates, and 3) the relation between reactive iron availability and pyrite formation to assess the buffering capacity of the sediments of the LSLE towards $\sum H_2S$. Based on previous studies, we expected to find an enrichment of AVS near the head of the LSLE where sedimentation rates are higher and bottom-waters are more

oxygen-depleted, as more reactive iron is available to form AVS and the latter is less likely converted to pyrite due to its rapid burial and isolation from oxidizing species. By examining the interplay between oxygen levels, iron availability, and sedimentation rates, this research aims to better understand the factors that influence diagenetic sulfur cycling in hypoxic environments.

Although the distribution of buried sulfur species alone cannot fully capture the complexity of the sulfur cycle's response to deoxygenation, it offers valuable insights into the balance of oxidation-reduction processes in sediments and the potential buffering capacity of these systems against the accumulation of porewater $\sum H_2S$ and its potential diffusion to the overlying waters.

1.4 MATÉRIAL AND METHODS

1.4.1 Study site

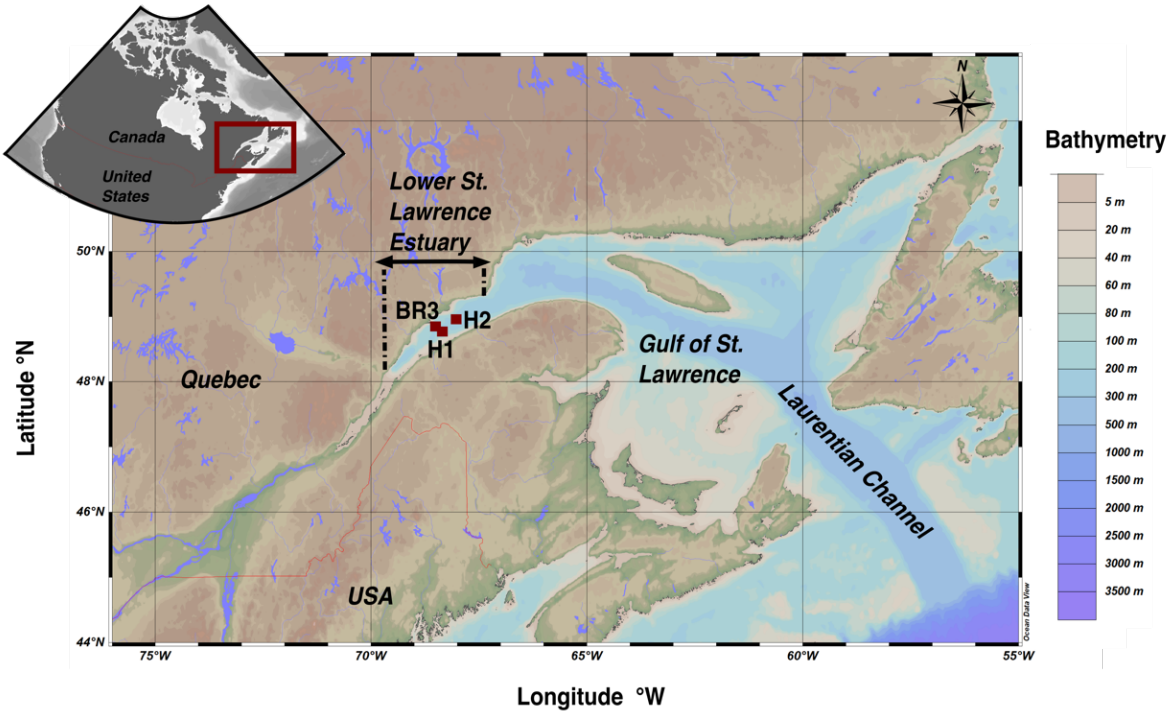

Fig 6 : Map of the St. Lawrence Estuary and Gulf with location of the study sites (BR3, H1 and H2) in the Laurentian Trough (see Table 2 for precise location and bottom-water properties). The cores were collected in 2022 and 2023.

The Lower St. Lawrence Estuary (LSLE) extends from Tadoussac to Pointe-des-Monts, where it opens into the Gulf of St. Lawrence (GSL). The Laurentian Trough is the main bathymetric feature of the LSLE and GSL. It is a 250-350 m deep submarine U-shaped valley excavated by Quaternary glacial erosion (King and Maclean, 1970). The channel extends from the eastern North American continental shelf break to Tadoussac at the head of the LSLE, where the seabed rises to 20 m (Belzile et al., 2016). The LSLE is characterized by estuarine circulation with three distinct layers in the water column during the ice-free season. These layers are thermally stratified, wherein brackish water flows seaward at the surface (0 to 30 m) over the cold intermediate layer (30 to 150 m; S_p = 32.0 to 32.6, where

S_p stands for practical salinity) that flows landward and is formed in the wintertime in the GSL (Galbraith, 2006). The warmer (~ 7°C) deep layer (>150 m; S_p = 33 to 35) also flows landward, bringing seawater from the Northwest Atlantic Ocean through Cabot Strait (Dickie and Trites, 1983, Jutras et al., 2023). The mean deep-water flow is estimated at ~0.5 cm s^{-1} (or 160 km yr^{-1}) (Bugden, 1991; Gilbert, 2004; Stevens et al., 2024). Therefore, waters entering the GSL through Cabot Strait take 2 to 5 years to reach the head of the channel (Bugden, 1991; Drinkwater and Gilbert, 2004; Gilbert et al., 2005; Stevens et al., 2024). Recent changes in the Northwest Atlantic Ocean circulation have impacted the LSLE's deep-water properties, as increasingly more oxygen-depleted and warmer water originating from the North Atlantic Central Waters contribute to the deep-water mass at the expense of the previously prevalent well-oxygenated and cold Labrador Current waters (Jutras et al., 2020, 2023a, 2023b). The depth of the channel, coupled with the strong stratification due to the estuarine circulation, isolates the bottom-waters from the atmosphere, allowing for their persistent deoxygenation, acidification and warming over the past century (Gilbert et al., 2005; Thibodeau et al., 2010; Mucci et al., 2011; Nesbitt and Mucci, 2021; Claret et al., 2018; Jutras et al., 2020, 2023a).

The sediments of the LSLE are iron-rich (Loring and Nota, 1968; Gagnon et al., 1995; Gobeil, 2006). The iron mainly originates from the weathering of rocks in the Canadian Shield rocks, including Grenvillian metamorphic rocks that are rich in amphiboles, potassium feldspar, plagioclase feldspar, and magnetite (Jaegle, 2015; Loring and Nota, 1973). In addition, the erosion of the Appalachian sedimentary rocks from the south shore of the LSLE, comprised of quartz and phyllosilicates, contributes to the sediments (Loring and Nota, 1973; Jaegle, 2015; Casse et al., 2017). The sediments of the Laurentian Trough consist of clay (60%), silt (35%), and sand (5-10%) (Loring and Nota, 1968). The clay fraction encompasses minerals such as amphiboles, feldspars, pyroxenes, chlorite, quartz, illite and kaolinite (Loring and Nota, 1968; Ramachandran, 1991; Casse et al., 2017). In addition to reactive detrital and authigenic oxides, including nanoparticulate goethite (Poulton and Raiswell, 2005; Van der Zee et al., 2003), ferric iron is also associated with silicate minerals (chlorite and illite) and well as poorly sulfide-reactive iron oxides such as magnetite (Nota and Loring,

1968; Ramachandran, 1991; Poulton and Canfield, 2005). The sedimentation rate is high in the LSLE, ranging from ~0.70 ± 0.03 cm a^{-1} near the head of the Laurentian Trough to ~0.11 ± 0.03 cm a^{-1} in the GSL (Audet et al., 2023; Genovesi et al., 2011; Thibodeau et al., 2006, Smith and Schafer, 1999; Silverberg, 1978).

Given its geological configuration and water mass characteristics, the LSLE serves as an exceptional natural laboratory for the investigation of geochemical transformations in a persistently saline, hypoxic, and iron-rich sedimentary environment.

1.4.2 Sampling Method

The water column and sediments at three sites were sampled in the Laurentian Trough, between Rimouski on the south shore and Baie-Comeau on the north shore, during two cruises aboard the *R/V Coriolis II* in May 2022 and May 2023 (Fig. 1). The sites were characterized by similar bottom-water practical salinity and depth (Table 1). At all three sites, $[DO]_{bot}$, was lower than the hypoxic threshold of 62.5 µM (Diaz and Rosenberg, 2008), as they were 34 µM, 36 µM, and 50 µM at sites H1, BR3, and H2, respectively.

Table 2 : Characteristics of the sampled sites in the LSLE in 2023 including water depth, bottom-water oxygen concentration 10 m above the SWI and practical salinity.

Station	Latitude (°N)	Longitude (°W)	Water depth (m)	$[O_2]_{bot}$ (µM)	S_p
BR3	48,84	68,48	353	36	34.6
H1	48,80	68,40	364	34	34.6
H2	48,96	68,03	303	50	34.6

Water samples were recovered from discrete depths throughout the water column with 12 L Niskin bottles mounted on a rosette sampler fitted with a Conductivity-Temperature-

Depth sensor (CTD Seabird® SBE 911plus) and oxygen probe (Seabird® SBE-43). Although the probes were calibrated by the manufacturer during the winter months preceding the cruises, discrete samples were taken from the Niskin bottles for on-board dissolved oxygen [DO] Winkler titrations, as described in Grasshoff et al. (1999), and the CTD records re-calibrated post-cruise. The bottom-water data presented in Table 1 were recorded 10 m above the sediment-water interface. The CTD was deployed before the sediment box corer to avoid the impact of sediment resuspension on water column properties.

In 2023, sediment cores were collected within a 50 m radius at the same sites (BR3 and H1) as those taken the previous year (Fig. 1). In 2023, a supplementary site, H2, was added (Fig. 1). Given the potential loss of the first 20 cm of sediment upon impact of the gravity corer, a box corer was first deployed to retrieve the undisturbed sediment-water interface. Depths equivalences from the box cores and the gravity cores were established using the porewater sulfate profiles.

Undisturbed sediment cores were retrieved with an Ocean Instrument Mark II box corer. Immediately after core (0.30 m^2 x 60 cm long) recovery, each box core was sub-sampled with three (3) Plexiglas push-core liners (10 cm ID) using a vacuum pump to avoid compression of the sediment. The first push-core was sub-sampled immediately after recovery with 20 mL cutoff syringes at 4-cm intervals for the first 10 cm and 5-cm intervals between 10 and 50 cm for analysis of the solid sediment reactive iron, AVS, and pyrite contents. After sub-sampling, the syringes were closed with Parafilm M® and sealed with electrical tape to avoid oxidation. They were stored in a hermetic jar with an AnareoPack™, an anoxic pack made of organic acid that generates CO^2, and frozen at -20°C. The second push-core was kept at 4°C for further analyses, including determinations of porosity, sedimentation rate using ^{210}Pb in excess and organic carbon (C_{org}) content.

The third push-core, destined for porewater extraction, was pre-drilled at 2-cm intervals over the first 10 cm and 5-cm intervals between 10 and 50 cm. The push-core was placed vertically in a custom-built wooden support. The 1-m gravity core sections were placed horizontally, and holes were drilled every 20 cm. Porewater extraction was performed with

individual *Rhizon*® (5-cm long inert porous polymer tubes with a pore size of 0.1 μm) probes introduced in each hole and connected to a 20 mL syringe to create a vacuum. One mL of the extracted porewater from each depth interval was transferred to a microcentrifuge tube for sulfate analysis. The porewater samples were stored at 4°C while onboard ship and later transferred to the Institut des Sciences de la MER (ISMER) laboratory without being exposed to ambient temperature for more than thirty minutes. The frozen sub-samples were transferred to a -20°C freezer at the ISMER laboratory as soon as we returned to shore. At each site, solid phase and porewater extraction were carried out on each gravity core (length from 168 cm to 190 cm and 10 cm ID) as described above for the push-cores, except that they were all carried out on the same core and at 20-cm intervals. After sub-sampling and porewater extraction, the gravity core was also kept at 4°C for further analyses, including determinations of porosity, sedimentation rate using ^{210}Pb and organic carbon (C_{org}) content. A summary of the core types sampled, and analyses performed at each site can be found in Table 3.

Table 3. Summary of the analyses performed in 2022 and 2023 on gravity cores and push-cores recovered from each sampling site

Site	Year	Core type[1]	Porosity	Sedimentation rate	C_{org} and $\delta^{13}C_{org}$	AVS and pyrite	Porewater Sulfate	Solid Reactive Iron
BR3	2022	GC	A[2]	-	-	-	A	-
		PC	A	A	-	-	A	-
	2023	GC	-	-	-	-	-	-
		PC	-	-	A	A	-	A
H1	2022	GC	A	-	-	-	A	-
		PC	A	A	-	-	A	-
	2023	GC	-	-	A	A	-	A
		PC	-	-	A	A	-	A
H2	2022	GC	-	-	-	-	-	-
		PC	-	-	-	-	-	-
	2023	GC	A	-	A	A	A	A
		PC	A	A	A	A	A	A

[1]Core types are GC for gravity core and PC for push-core

[2]A stands for analysis performed

1.4.3 Porosity

The porosity, water content, and dry density of sediment samples recovered from the gravity and push-cores were determined. After returning to the laboratory, the cores kept at 4°C were opened on a laboratory bench, and exactly 2 mL of wet sediment were sampled with a cut-off syringe, transferred to porcelain crucibles, and weighed on an analytical balance. The sediment was then dried in an oven at 55°C for 24 to 48 hours. The dry samples were weighed again, and the difference was calculated to obtain the water content.

The percent water content (W_c) was calculated as follows:

$$W_c = \frac{(m_w - m_{sed})}{m_w}\ x\ 100 \qquad (4)$$

where m_w is the mass of wet sediment and m_{sed} is the mass of dry sediment. The porosity (ϕ) was calculated according to:

$$\phi = \frac{interstitial\ volume}{total\ volume} = \frac{\frac{m_{pw}+m_s}{\rho_{pw}}}{\frac{m_{pw}+m_s}{\rho_{pw}}+\frac{m_{sed}}{\rho_{sed}}} \qquad (5)$$

where m_{pw} is the mass of porewater (calculated by multiplying m_w by W_c divided by 100), m_s is the mass of salt (calculated from the bottom-water salinity), ρ_{pw} is the porewater density (1.025 g∗cm^{-3}), m_{sed} is the mass of dry sediment and ρ_{sed} is the density of sediment (estimated at 2.65 g∗cm^{-3}).

1.4.4 ^{210}Pb in excess measurements

The age models were established from vertical profiles of the ^{210}Pb in excess measurements for cores BR3, H1, and H2. Measurements were carried out at the GEOTOP facilities (Radiochronology laboratory, GEOTOP-UQÀM, Montreal, Quebec, Canada) at

least 6 months after recovery of the cores. The ^{210}Pb activity in the sediment was obtained indirectly by measuring the decay rate of its daughter isotope ^{210}Po ($t_{1/2}$ = 138.4 days; α = 5.30 MeV) by alpha spectrometry, assuming secular equilibrium. To determine the extraction and counting efficiency as well as to measure the decay rate, about 0.1 g of ^{209}Po was added to the freeze-dried samples as a spike (Flynn 1968). The samples underwent a series of acid digestions (HCl: HNO_3, hydrofluoric acid, and H_2O_2), and the purified polonium was deposited on a silver disk. The $^{209\text{-}210}$Po activities were measured in a silicon surface-barrier multichannel α-spectrometer (EGG-ORTEC, type 576A) paired with a MAESTRO Multichannel Analyzer Emulation Software. Uncertainties were estimated from counting statistics to be approximately 6% for two standard deviations (2σ).

1.4.5 Elemental and isotope composition of the sediment

The total carbon (C_{tot}) and organic content (C_{org}) of the sediments were measured at the GEOTOP facilities (Light stable isotope geochemistry laboratory, GEOTOP-UQÀM, Montreal, Quebec, Canada) by high-temperature catalytic combustion with an elemental analyzer (Carlo Erba NC2500) coupled to a gas chromatograph equipped with a thermal conductivity detector. For the determination of C_{org}, 7-8 mg of the freeze-dried sediment samples were weighed in a silver capsule, transferred to a Teflon holding plate, and inserted in a closed container in the presence of concentrated HCl for 24h to decarbonate the samples (Hélie, 2009). Inorganic carbon (C_{inorg}) was determined from the difference between C_{tot} and C_{org}. The organic carbon isotopic composition ($\delta^{13}C_{org}$) was determined on the decarbonated samples with a continuous flow isotope ratio mass spectrometer (Isoprime 100 Microcube) coupled to an elemental analyzer (Vario-Isotope cube). Carbon isotope ratios are reported in the δ notation per mil (‰) relative to the Vienna Pee Dee Belemnite (V-PDB) standard. Two internal reference materials ($\delta^{13}C$= -28.74 ± 0.02‰ and -11.80 ± 0.03‰) were used to normalize the results on the NBS19-LSVEC scale. A third reference material ($\delta^{13}C$= -17.06 ± 0.02‰) was analyzed as an unknown to assess the exactness of the normalization. The

standard deviations (± 1σ) for the C_{org} and $\delta^{13}C$ analyses were generally better than 0.15% and 0.1‰ respectively, based on replicate measurements of organic standard substances.

1.4.6 Acid volatile sulfides (AVS) and pyrite extractions

The AVS and reduced sulfur in pyrite were extracted following the two-step distillation method described by Fossing and Jørgensen (1989). AVS (mainly Fe monosulfides; FeS) were distilled first with 6 N HCl, and then chromium(II) was added to release the chromium reducible sulfides contained in pyrite (FeS_2). A 6-position extraction line was used for sample processing. First, frozen wet samples in cut-off syringes were removed from the freezer and allowed to thaw for 5 minutes so the sediment was soft enough to be pushed out of the syringe. Sub-sampling, thawing, and weighting were conducted on the counter to minimize exposure time to the atmosphere (~3-5 min). Approximately 1.5 g of wet sediment were weighed in a three-necked round flask, and the flask rapidly transferred into an inert nitrogen atmosphere. To extract the AVS, 20 mL of 6N HCl solution was first added to the flask. Stirring (~250 rpm) and heating (~70°C) were used to accelerate the reaction that was carried out for 1 h.

The hydrogen sulfide (H_2S) extracted from the AVS distillation was carried by a stream of nitrogen (N_2) gas to a 50 mL Falcon tube containing 15 mL of a 5% zinc acetate (ZnAc) in 3% glacial acetic acid (HAc) solution. After 1 h of extraction, 10 mL of anoxic chromium(II) solution was added to the distillation flask to extract the reduced sulfur in pyrite and the released H_2S was carried by a stream of N_2 and captured in a second 50mL Falcon tube containing a fresh 5 % ZnAc 3 % acid glacial HAc solution. This second extraction was carried out for 1.5 h, with continuous stirring (~250 rpm) and heating (~70°C for the first 30 min, lowered to ~30° for the next hour). The H_2S trapped in the Falcon tubes was converted to ZnS, that can be measured by spectrophotometry.

The amount of ZnS contained in the traps was then quantified by spectrophotometric analysis following the methylene blue method of Cline (1969) in 1-cm spectrophotometric glass cuvettes, and the absorbance was measured at the absorbance peak of the color complex, 672 nm. The linear range of the method was established with gravimetrically prepared standard zinc sulfide solutions and was between absorbances of 0.1 and 0.8, corresponding to sulfide concentrations of 2 µM to 18 µM. Samples with higher concentrations were diluted to fit within the linear range of the spectrophotometric analysis. To verify the results obtained by the colorimetric method, an iodometric titration method was also used (Canfield et al., 1986; Lefort et al., 2012). The stock solution used to construct the spectrophotometric method calibration curve was back-titrated idiometrically with an automatic titrator (Metrohm 775 Dosimat).

The AVS and Fe_{pyr} contents as well as the AVS-S:pyrite-S ratios were calculated from the measured sulfide content of each sample, assuming a 1:1 Fe:S stoichiometry for AVS and a 1:2 Fe:S stoichiometry for the pyrite. The percentage of recovery based on a 99% pyrite standard was above 95% and the average standard analytical error based on linear regression of the calibration curve of the standards was ± 0.2 µmol of S/g of dry sediment. Given the heterogeneity of the sediments, the average estimated uncertainty for 15 replicates was 40% of dry sediment.

1.4.7 Porewater sulfates

Porewater sulfate concentrations were quantified using ion chromatography (IC) on a Dionex system utilizing an AG-18/AS-18 column (250 mm Thermo Scientific Dionex IonPac™) with a KOH eluent. To achieve good separation of the sulfate from the chloride ions, the eluent concentration was kept at 12 mM until the sulfate peak was eluted. The eluent concentration was then increased to 30 mM KOH to flush the column of strongly bound ions. Because salinity has an important impact on the results, calibration standards matched the seawater salinity of the samples, allowing for the measurement of sulfate concentrations

ranging from 0 to 0.28 mM. Samples were diluted 1:100 to fit within the calibration curve. The concentrations were calculated using a peak integration method and reported in porewater concentrations after correction for the dilutions. The precision of the analysis was established by replicate measurements of standards prepared in laboratory matching the salinity of the samples. The standard deviation of the analyses was 5%.

1.4.8 Reactive solid iron extractions

Iron speciation was determined on wet sediment samples according to a sequential extraction protocol described by Poulton and Canfield (2005) and Laufer et al. (2019). The designated reactive iron pool (Fe_R) encompasses the dithionite-soluble (oxyhydr)oxides such as ferrihydrite, lepidocrocite, goethite and hematite, in addition to the iron that was transformed to pyrite, according to the definition of highly reactive iron of Poulton and Canfield (2005). In this study, it also encompasses the poorly reactive magnetite (Fe_{mag}) that can react with sulfide on a several hundred-year timescale (Canfield and Berner, 1987). The extraction was carried out on 50 to 150 mg of wet-weight sediment samples. The sequential extraction includes three steps summarized in Table 4 The first extraction is carried out with a 0.5 N HCl and hydroxylamine-HCl solution that extracts easily reducible and poorly crystalline Fe(III) (e.g., ferrihydrite, lepidocrocite, nanoparticulate goethite) along with the Fe(II) in AVS, carbonates and phosphates. In this study, the Fe(II) associated with AVS is subtracted from the first extraction step to obtain the term easily reducible oxides (Fe_{ox1}) component, as defined by Poulton and Canfield (2005). The second extraction is carried out with a 50g/L Na-dithionite solution (buffered with 0.2 M sodium citrate and 0.35 M acetic acid to pH 4.8) that extracts reducible crystalline Fe(III) (mostly goethite, hematite, and some magnetite) (Fe_{ox2} – reducible oxides according to Poulton and Canfield (2005)). The last extraction is carried out with a 0.2 M ammonium oxalate/0.17 M oxalic acid solution (buffered with ammonium hydroxide to pH 3.2) that extracts magnetite (Fe_{mag}). The amount of iron released from each of the three extractions was determined by the ferrozine

colorimetry method (UV-Vis spectrophotometer at 561 nm) (Stookey, 1970). An aliquot of the extracts was also reacted with a hydroxylamine reductant to reduce Fe(III) to Fe(II) and the ferrozine analysis was repeated. Hence, the Fe(III) content was determined from the difference between the "total" extracted Fe (Fe(III) + Fe(II)) and Fe(II). Because the hydroxylamine reductant interferes with the spectrophotometric analysis, calibration curves were constructed with hydroxylamine and without hydroxylamine, depending on the extraction method. The reactive Iron (Fe_R) is equal to the sum of all the extracted iron pools minus Fe_{AVS} (i.e., $Fe_R = Fe_{ox1} + Fe_{ox2} + Fe_{mag} - Fe_{AVS}$). The sediment is inherently heterogeneous and, thus, it was necessary to establish the uncertainty of the measurements. To do so, triplicates sediment samples from fifteen core depths were measured. The variability in triplicate measurements was between 7% and 62%, with a mean of 25%.

Table 4. Sequential extraction of reactive iron (Fe_R)

Step	Extractant - duration	Operational definition
1	0.5 N HCl -1h + HAHCl 10% (w/v)	Fe_{ox1}
2	Na-dithionite/citrate pH 4.8	Fe_{ox2}
3	Ammonium oxalate/oxalic acid pH 3.2	Fe_{mag}

The degree of pyritization (DOP) is a parameter used to distinguish between sedimentary environments where pyrite formation is either sulfide or iron-limited (Raiswell and Berner, 1985). High DOP values are associated with euxinic conditions where bottom-waters are anoxic and contain plentiful or excess $\sum H_2S$ (Raiswell and Berner, 1985). DOP is calculated from the molar concentration ratio of pyrite-iron to the total reactive solid iron (Fe_R) in the sediment, where FeS_2-S is the concentration of reduced sulfur in pyrite:

$$\text{DOP (\%)} = \frac{0.5FeS_2}{0.5FeS_2 - S + Fe_R} \text{ x } 100$$

The DOP estimates are strongly dependent upon the operational definition of the reactive mineral iron (Raiswell et al., 1994). In earlier studies of the LSLE, the amount of reactive mineral iron was quantified following a 1N HCl extraction procedure (Gagnon et al., 1995). It has been suggested that this method can underestimate the goethite and hematite contents (Raiswell et al., 1994). On the other hand, the dithionite extraction can overestimate the amount of reactive iron by extracting AVS (Raiswell et al., 1994). To avoid this overestimation, we subtracted Fe_{AVS} from Fe_R. We also decided to only compare our DOP values with those of a study that followed the same extraction protocol for the reactive solid iron, AVS, and pyrite (Liu et al., 2021).

1.5 RESULTS

1.5.1 Sedimentation rates and age models

Sedimentation rates were estimated using the ^{210}Pb-decay constant (λ), the linear least-squares regression slope of the logarithmic function of the excess ^{210}Pb, and the Constant Flux (Constant Rate of Supply) model with Monte Carlo uncertainty under the assumption of a constant rate of supply. Excess ^{210}Pb was calculated by subtracting supported ^{210}Pb, determined by taking the three lowest ^{210}Pb activities for the deepest samples. To define the age models, the Plum package (Aquino-López et al., 2018) within the R environment (R core Team, 2021) was used, accounting for the total ($^{210}Pb_{tot}$) and supported ($^{210}Pb_{sup}$) ^{210}Pb activities, the density (g/cm^{-3}) of samples, and the coring date. Uncertainties for the sedimentation rates were calculated based on the standard deviation of the slope.

The Ln(^{210}Pb excess) data at the three sites were fitted to simple linear least-squares regressions. The slopes at BR3, H1 and H2 were, respectively, -0.09 ($F_{1,20} = 149.2$, $p = 9.959\text{x}10^{-11}$; Fig. 6A), -0.07 ($F_{1,18} = 195.1$, $p = 4.231\text{x}10^{-11}$; Fig. 6B) and -1.5 ($F_{1,7} = 128.8$, $p = 9.226\text{x}10^{-6}$; Fig. 6C), corresponding to sedimentation rates of, respectively, 0.3 ± 0.03 cm yr^{-1}, 0.4 ± 0.03 cm yr^{-1} and 0.2 ± 0.02 cm yr^{-1} (Fig. 6C).

Assumptions used to set a chronology are 1) a constant flux of ^{210}Pb and 2) a uniform sedimentation rate throughout the cores, expanding to the results obtained in the first 50 cm up to 200 cm.

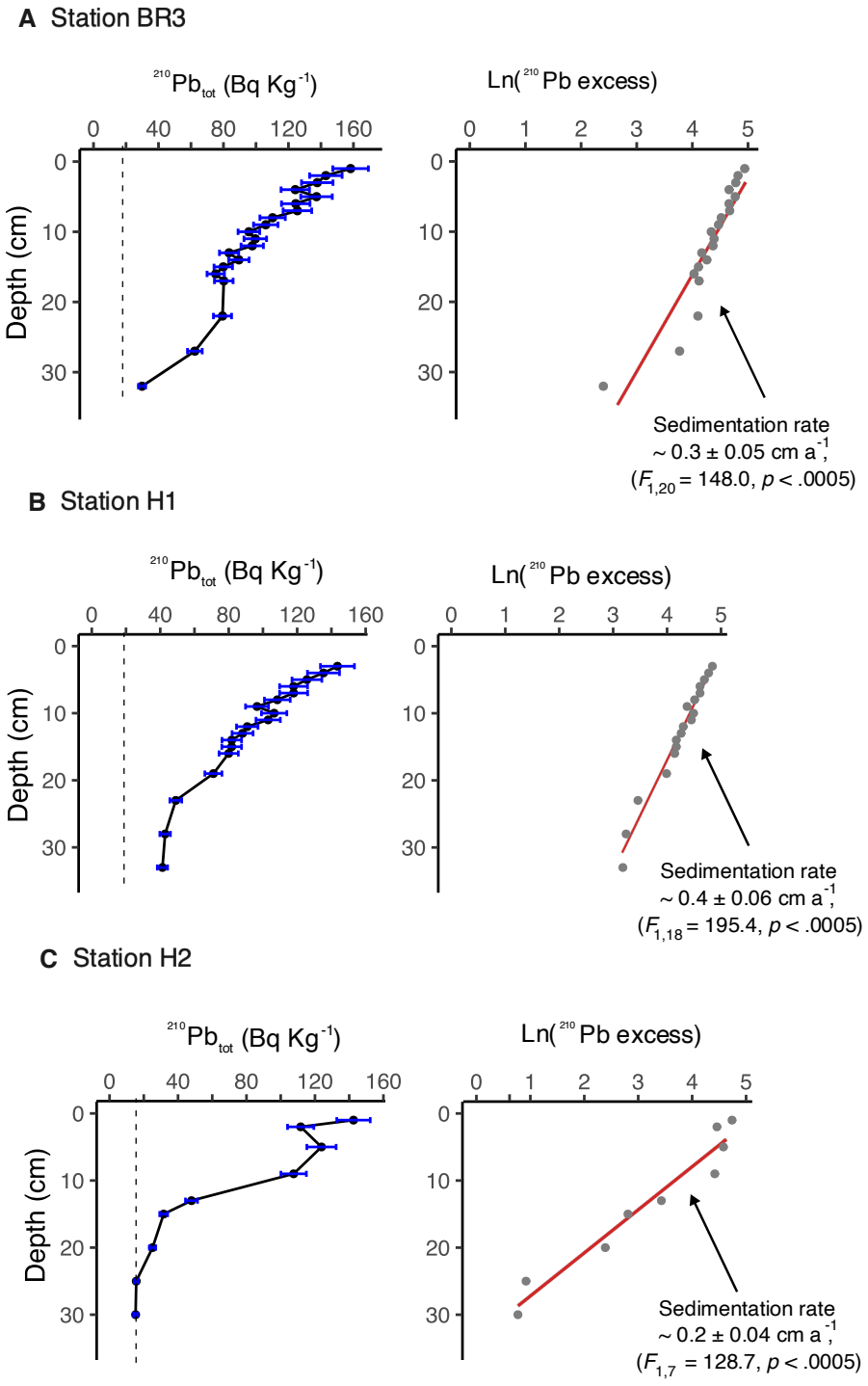

Figure 7. Excess ^{210}Pb (ln) at **A:** site BR3, **B:** site H1, and **C:** site H2. The vertical dotted line represents the supported ^{210}Pb value estimated from data at the bottom of the cores. Sedimentation rates were calculated from a least-squares linear regression

1.5.2 Sediments characteristics

The sedimentary organic carbon content (%C_{org}) in the cores recovered at the three study sites ranges from 0.53% to 1.84% (dry weight) (Fig. 2). The organic content of the surface sediments (i.e., 0-1 cm) at site BR3 and H1 is very similar 1.80% and 1.75%, respectively, but is slightly lower (1.42%) at site H2. It typically decreases with depth in all three cores, with a very similar trend at sites BR3 and H1 over the first 50 cm, but decreases faster and to a lower value at site H2, reaching ~1.00% at around 25 cm depth, compared to ~1.25% at the same depth at sites BR3 and H1. These values do not necessarily translate into faster mineralization rates because of the lower sedimentation rate at site H2. There also appears to be a break in the profiles at different depths at H1 (~125 cm, 312 ± 48 years) and H2 (~45 cm, 225 ± 47 years). Given the uncertainties in the age model, the breaks could be associated with the same event.

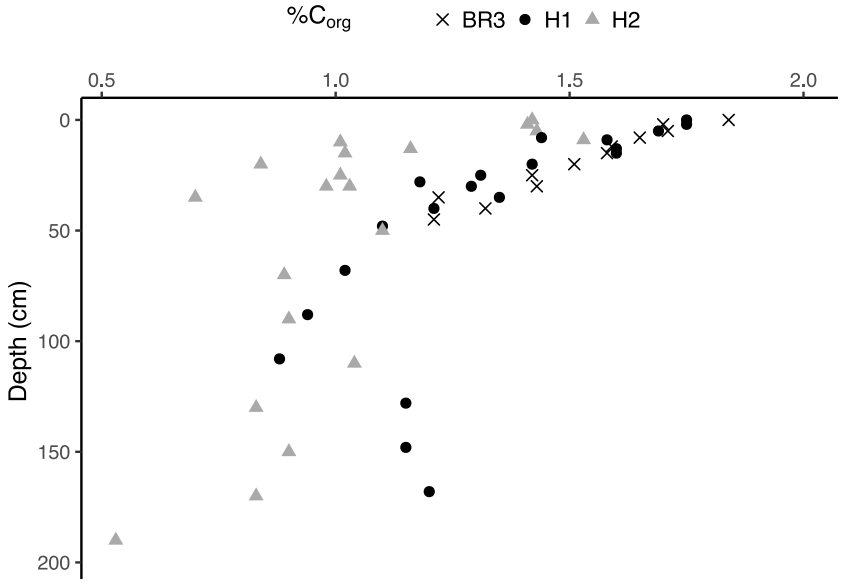

Figure 8 Vertical distribution of organic carbon (weight %) in the sediments at sites BR3, H1, and H2 in the LSLE. Only data from 2023 are reported here

The $\delta^{13}C_{org}$ data show similar signatures at sites BR3 and H1 and a slightly distinct one at site H2 (Fig. 3). There is a gradual increase of $\delta^{13}C_{org}$ values with depth in the first 45 cm

of all three cores, corresponding to the push-core lengths. At site BR3, the $\delta^{13}C_{org}$ values fluctuate between -24.1‰ and -24.6‰ throughout the core (i.e., from 0 to 45 cm). At sites H1 and H2, values range respectively from -26.2‰ to -24.2‰ and from -24.1‰ to -23.5‰ in the upper section (0-45cm); whereas, in the lower section (45-168 cm), they vary respectively from -25.4‰ to -23.9‰ and from 24.2‰ to -23.6‰. They reflect the slightly higher proportions of terrestrial versus marine organic matter at the upstream sites in the LSLE. Two anomalous, episodic, and higher terrigenous inputs seem to be recorded at H1, the first one around 12 cm depth (-26.7‰ at 9 cm depth, -25.7‰ at 15 cm depth) and the second one at 108 cm depth (-25.4‰).

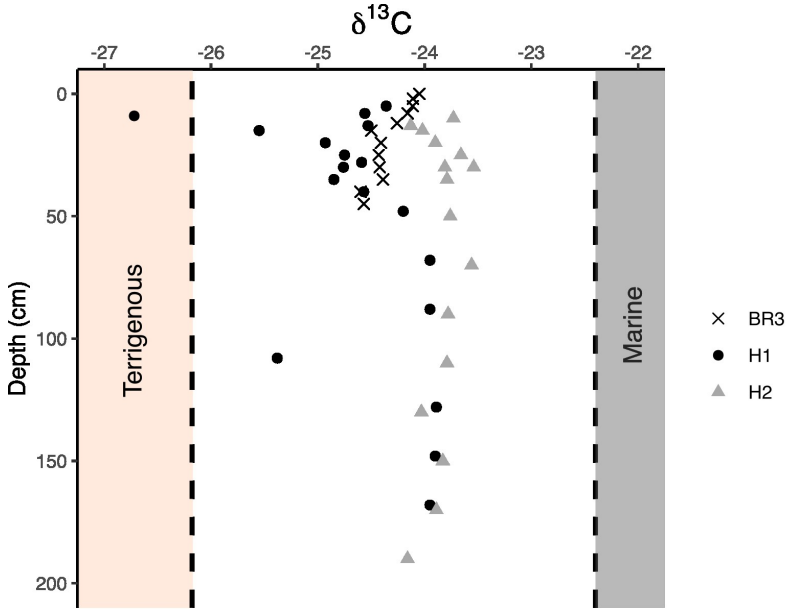

Figure 9. Vertical distribution of $\delta^{13}C_{org}$ in the sediments at sites BR3, H1, and H2. Dashed lines represent the terrigenous (-26.18 ± 0.65‰, average of river (-26.26 ± 0.39‰; Hélie and Hillaire-Marcel, 2006), and soil (-26.10 ± 0.76‰; Douglas et al., 2022) OC), as well as the marine (-22.44 ± 1.44‰; Yves Gélinas, pers. comm.) endmembers in the LSLE

1.5.3 AVS, pyrite, and sulfates

The vertical AVS and pyrite profiles at sites BR3 and H1 show a similar trend (Fig. 6), whereas the AVS profile at site H2 is nearly featureless. Specifically, AVS concentrations increase from undetectable concentrations at the sediment-water interface (SWI) in all cores and peak at 26 μmol/gdw (dried sediment) at a depth of 25 cm at BR3 and 31 μmol/g (dried sediment) at 30 cm at H1 (Fig. 6). In contrast, AVS concentrations are low at site H2, reaching only 6 μmol/g (dried sediment) at a depth of 15 cm. The pyrite concentrations at sites BR3 and H1 exhibit a parallel trend, progressively increasing from undetectable concentrations at the SWI to 20 μmol/g (dried sediment) at 45 cm depth at BR3 and 24 μmol/g (dried sediment) at 40 cm depth at H1. Conversely, pyrite concentrations at site H2 rise to 62 μmol/g (dried sediment) at 50 cm depth. In the lower part of the cores, below 50 cm, pyrite concentrations at sites H1 and H2 increase similarly, reaching a maximum of 70 μmol/g (dried sediment) at 128 cm depth at site H1 and 98 μmol/g (dried sediment) at 170 cm depth at site H2.

The porewater sulfate concentrations at all three sites show a similar depth trend. They are close to the overlying seawater value (~28 mM) at the SWI and decrease below a 15 cm depth. At depth, the sulfate concentrations decrease more sharply at BR3 and H1 than at H2, reaching 8.4 mM by 229 cm depth at BR3, 7.9 mM by 172 cm depth at H1 and 19.5 mM by 199 cm depth at H2 (Fig. 10).

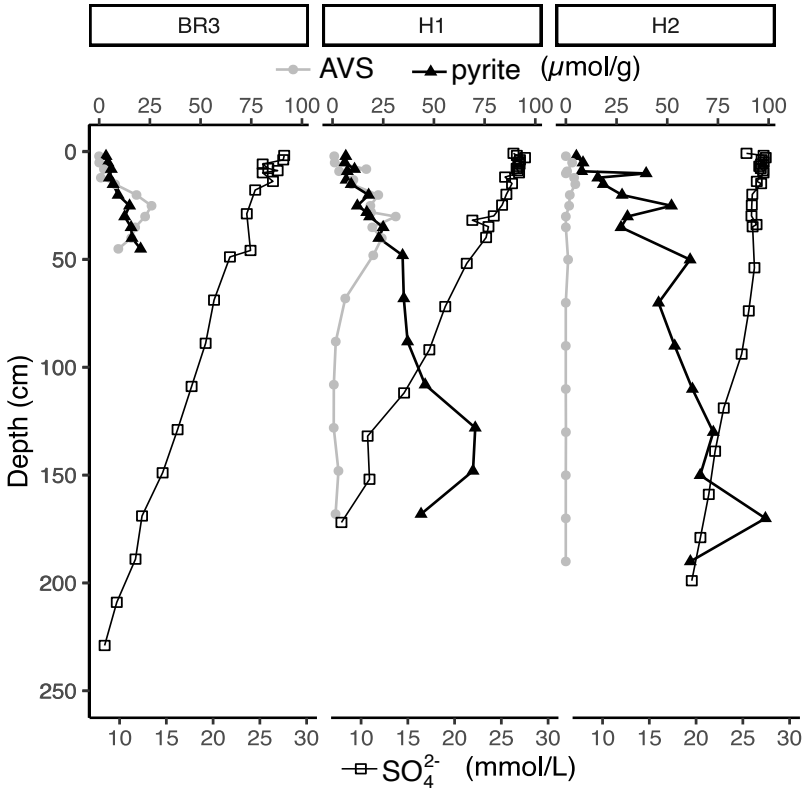

Figure 10. Vertical profiles of AVS, pyrite, and porewater sulfate concentrations at sites BR3, H1, and H2. AVS and pyrite concentrations are in μmol/g of dry sediment

1.5.4 Reactive solid iron

The reactive iron (FeR) concentrations exhibit spatial variations, with more elevated content at BR3 and H1 than at H2 (Fig. 5). Specifically, the mean FeR concentration within the first 45 cm at site BR3 is ~370 μmol/g (dried sediment) whereas, it is ~400 μmol/g (dried sediment) at site H1. A lower mean concentration of ~290 μmol/g (dried sediment) is recorded in the first 45 cm at site H2. Similar trends are observed for Fe_{ox1}, representing the most reactive solid iron phase. In the upper 45 cm of sediments, the mean concentration of

Fe_{ox1} at site BR3 is ~170 µmol/g (dried sediment), ~220 µmol/g (dried sediment) at site H1, and ~130 µmol/g (dried sediment) at site H2.

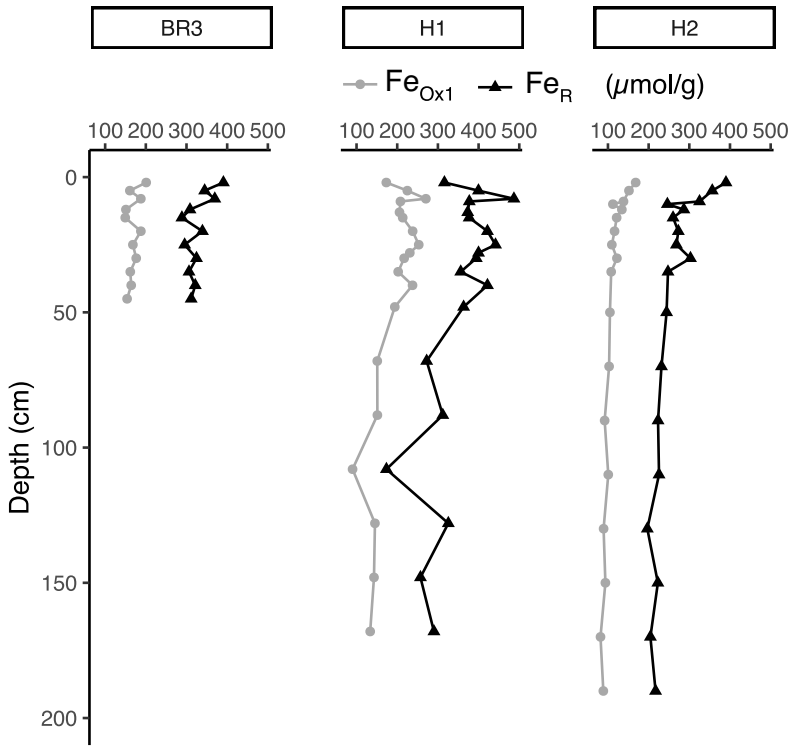

Figure 11 Vertical profiles of reactive iron (Fe_R) and easily-reducible, poorly crystalline, non-sulfur bound iron (Fe_{Ox1}). Concentrations are in µmol/g of dry sediment.

Below 50 cm, the FeR concentrations decrease progressively at H1 but are relatively invariant at H2. More specifically, the FeR concentration measured at 48 cm at H1 is ~360 µmol/g (dried sediment) and diminishes to ~290 µmol/g (dried sediment) at 168 cm, whereas, at H2, the FeR concentration decreases from ~250 µmol/g (dried sediment) at 50 cm to ~200 µmol/g (dried sediment) at 170 cm

1.6 DISCUSSION

The worsening, persistent bottom-water hypoxia in the LSLE (Jutras, 2023, 2020) has prompted changes in the environment and the benthic ecosystem (Belley et al. 2010, Pascal et al., 2024). These changes include a modification of the biogeochemical cycles within the sediments, including the sulfur cycle as sulfate-reduction rates and the production of ∑H2S are expected to increase (Katsev et al., 2007). Modifications of the geochemical cycles of redox-sensitive elements in the sediment have already been reported, with a redistribution of solid phases, specifically reactive iron phases, and trace elements (e.g., As) (Lefort et al., 2012). The response of geochemical cycles to persistent hypoxia, however, is non-linear in the LSLE (Katsev et al., 2007; Pascal et al., 2024), and the present study provides an opportunity to explore the differences in sulfur species distribution between three sites near the head of the Laurentian Channel and within 10 km radius of each other.

1.6.1 Effects of environmental factors on spatial variation of the distribution of AVS and pyrite in the sediments

$[DO]_{bot}$ were under the hypoxic threshold of 62 µmol/L at the three studied sites, below which the activity of benthic and epibenthic organisms (bioturbation and bio-irrigation) is inhibited and, therefore, not expected to participate directly in the redistribution of redox-sensitive species and their diagenetic cycles (Pascal et al., 2024). Nevertheless, we observed spatial variations in the distribution of sulfur species buried in the sediments (Fig. 10, more specifically differences in the sediment accumulation rates of AVS and pyrite (Table 3). Porewater $\sum H_2S$ was not detectable in any of the sites and all sites also had high reactive solid iron content (200 µmol/g of dry sediment), consistent with results of previous studies (Lefort et al., 2012; Katsev et al., 2007; Sundby et al., 2004). The AVS-S-to-pyrite-S ratios were higher at the upstream sites, reaching 0.9 at sites H1 and BR3 but never exceeding 0.2 at site H2 (Table 3). Sedimentation rates were variable between sites, with a slightly higher sedimentation rate at site H1 (0.4 ± 0.03 cm yr^{-1}) and BR3 (0.3 ± 0.03 cm yr^{-1}) than at H2

(0.2 ± 0.02 cm yr^{-1}). The sedimentation rate obtained in this study at site H1 is identical to the one estimated by Thibodeau et al. (2006) at the same site from a core recovered in August 2000. It is lower than those estimated by Audet et al. (2023) and Smith and Schafer (1999) at site H1, where they were evaluated at 0.7 ± 0.03 cm yr^{-1}. The differences in sedimentation rates between site H1 and H2 are, however, consistent with results of previous studies where a site close to H2 had a sedimentation rate ~1.5 cm yr^{-1} lower than a site close to site H1 (Smith and Schafer, 1999).

In the following sections, we will investigate the factors that could explain the observed differences in the solid, reduced sulfur species (AVS and pyrite) distributions in these iron-rich sediments. To do so, we first inventory the processes that control the S cycle in the LSLE sediments: organic matter burial, the iron diagenesis, and the re-oxidation processes of reduced species. All these processes are modulated by the sedimentation rate, and we propose to identify which factor had the strongest influence on the repartition of sulfur species in the sediments of the LSLE under the prevailing hypoxic conditions. We then evaluate the buffering capacity of the LSLE reactive solid iron pool toward porewater $\sum H_2S$ accumulation.

Table 5. Surface sediment (0-1) organic carbon accumulation rates, mean sediment accumulation rates (SAR), inventories, average authigenic AVS and pyrite accumulation rates of over the upper 35 cm of each core, and the maximum AVS-S-to-pyrite-S ratio. All results are given relative to the number of moles of S.

	BR3	**H1**	**H2**
Surface sediment (0-1 cm) organic carbon accumulation rate (mg·C cm^{-2} yr^{-1})	2.6	4.3	1.9
Mean SAR (g cm^{-2} yr^{-1})	0.17	0.22	0.15
Mass of sediment accumulated over the length of the core (g cm^{-2})[a]	21	20.7	27.7
Time to accumulate 35 cm of sediments (yr)[b]	125	94	188
AVS inventory in 35 cm of sediments (µmol·S cm^{-2})[c]	275.8	331.0	45.5
AVS accumulation rate (µmol·S cm^{-2} yr^{-1})[d]	2.2	3.5	0.2
Pyrite inventory in 35 cm of sediments (µmol·S cm^{-2})[c]	411	574	1355
Pyrite accumulation rate (µmol·S cm^{-2} yr^{-1})[d]	**3.20**	**6.11**	**7.22**
Pyrite +AVS inventory in 35 cm of sediments (µmol·S cm^{-2})[c]	686	905	1400
Pyrite + AVS accumulation rates (µmol·S cm^{-2} yr^{-1})[d]	5.50	9.65	7.47
Maximum AVS-S-to-pyrite-S ratio	0.98	0.85	0.18

[a]Mass (g cm^{-2}) = $\sum(1-\phi)\rho\Delta 1$ where ϕ is the measured porosity, ρ is solid phase density (2.65), and $\Delta 1$is the thickness of the individual layer analyzed in cm.
[b]Time = accumulated mass (g cm^{-2}) / accumulation rate (g cm^{-2} yr^{-1}).
[c]Inventory =$\sum$(concentration)$(1-\phi)\rho\Delta 1$.
[d]Average accumulation rate = inventory / time

1.6.1.1 Control on the amount and reactivity of organic matter (OM) reaching the sulfate-reduction zone, controlling sulfate-reduction rate and the amount of $\sum H_2S$ produced

In marine environments, the rate of sulfate reduction (SRR) partly depends on the quantity and reactivity of the OM that reaches the anoxic zone after transiting through the oxic sediment layers (Goldhaber and Kaplan, 1975; Toth and Lerman, 1977; Berner, 1978). This sediment organic carbon content depends both on the origin and reactiviy of the organic matter that accumulates at the sediment surface and on the amount of organic matter mineralized by oxidants that precede sulfates in the sequence of catabolic reactions during early diagenesis.

The organic carbon content of the surface sediments (i.e., 0-1 cm) at site H2 was slightly lower ($\%C_{org}$ = 1.42%) than at BR3 ($\%C_{org}$ = 1.80%) and H1($\%C_{org}$ = 1.75%) (Fig. 2). According to the sediment accumulation rates and the C_{org} content at the surface, the C_{org} accumulation rate is the lowest at H2 site (1.9 mg·C cm^{-2} yr^{-1}). This indicates a lower input of organic matter at site H2. However, the $\delta^{13}C_{org}$ values indicate that there is a higher relative fraction of marine versus terrestrial organic matter reaching the sediment at H2 ($\delta^{13}C_{org}$ = -23.9‰) than at BR3 ($\delta^{13}C_{org}$ = -24.3‰) and H1 ($\delta^{13}C_{org}$ = -24.6‰) (Fig. 3). These results indicate that more marine, as opposed to terrestrial, organic carbon reaches the SWI as we move downstream in the LSLE. Hence, the reactivity of the sedimentary organic carbon deposited in at study sites presumably varies despite their proximity. These results are consistent with the trend reported in previous studies along the Gulf and St. Lawrence Estuary, with a transition from terrigenous at the head of the Trough to marine organic matter in the Gulf (Lucotte et al., 1991; Alkhatib et al., 2012).

The $[DO]_{bot}$ can also exert a control on the amount and reactivity of the organic matter reaching the sulfate reducing zone by impacting the depth of oxygen penetration and the oxygen exposure time, both a function of the $[DO]_{bot}$ and the sedimentation rate, and therefore the amount of organic matter remineralized by SR during early diagenesis (Cool, 2022). Although the $[DO]_{bot}$ concentrations at the three studied sites were below the hypoxic

threshold of 62 µM, it was slightly higher at the downstream site H2 than at BR3 and H1 (respectively 50, 36, and 34 µM) (Table 1). Recent research in the LSLE suggests that under the threshold value of ~54 µM of $[DO]_{bot}$, the aerobic degradation rate of organic matter in the sediments displays a non-linear response to deoxygenation to the benefit of anaerobic mineralization: DO being mainly consumed at the redox front to oxidize the reduced species (e.g., Mn(II), Fe(II), NH_4^+) diffusing from below (Katsev et al., 2007; Pascal et al., 2024). As site H2 was characterized by a slower sedimentation rate, lower organic carbon accumulation rate and a higher concentration of $[DO]_{bot}$, less reactive OM is expected to reach the sulfate-reduction zone. This is consistent with previous studies that showed a decreasing SRR downstream in the LSLE (Edenborn et al., 1987) (In this study, however, SRR was not estimated from sulfate profiles, as this method is based on sulfate transport by molecular diffusion and would likely underestimate transport by bio-irrigation (Jørgensen and Park 2010)). Considering these three factors, one would expect a lower production of $\sum H_2S$ at site H2 than at site H1 and BR3.

Nevertheless, differences in the amount of $\sum H_2S$ produced among the three sites are likely not sufficient to explain the discrepancies observed in the AVS-S-to-pyrite-S ratios (Table 5. Our results show that the pyrite accumulation rate is fastest at site H2 (7.2 µmol·S cm^{-2} yr^{-1}; Table 5. Likewise, the accumulation rate of solid reduced S in the sediments (AVS + pyrite) is greater at site H2 (7.4 µmol·S cm^{-2} yr^{-1}; Table 5) than at site BR3 (5.5 µmol·S cm^{-2} yr^{-1}; Table 5). These results suggest that there is enough $\sum H_2S$ production at site H2 to form pyrite. Therefore, the differences observed among the closely located sites and the quasi-absence of AVS at site H2 cannot be explained solely by the presumably lower sulfate reduction rate at this site, as was suggested by Sundby et al. (2004) when comparing the AVS content between a site at the head of the Trough and sites in the Gulf. The iron content is likely another environmental factor that can modulate the formation of AVS is the iron content.

1.6.1.2 Control on the amount of reactive iron, determining the extent of AVS precipitation

Whereas SRR and ∑H2S production are critical for AVS formation, the availability of reactive iron is equally important in determining the fate of sulfur species in the sediments. In iron-limited environments, increased SRR can lead to the buildup of porewater $\sum H_2S$ concentrations, enhancing the conversion of AVS to pyrite through the "H2S pathway" where AVS react with $\sum H_2S$ to form pyrite (Goldhaber and Kaplan, 1974; Jørgensen, 1977,1982,1990; Raiswell et al., 1988; Lyons, 1997). In the iron-rich sediments of the LSLE, however, pyrite formation likely proceeds only via the "polysulfide pathway", where AVS react with intermediate oxidative S species produced by the partial oxidation of reduced sulfur by a variety of oxidants (oxygen, Mn(IV), Fe(III)), to form pyrite (Gagnon et al., 1995, 1996).

In all studied cores, porewater $\sum H_2S$ concentrations were below our detection limit (<50 µM (data not shown)) all along the sediment cores. These results indicated that $\sum H_2S$ produced by sulfate-reduction was either oxidized or precipitated as AVS upon production, preventing any significant build-up in the porewaters (Boesen and Postma, 1988; Gagnon et al., 1995). Furthermore, all sites studied showed elevated concentrations of reactive solid iron (FeR) in the first 50 cm (>200 µmol/g; Fig. 5), in agreement with results reported in the same area (Ramachandran, 1991; Gagnon et al., 1995; Sundby et al., 2004; Katsev et al., 2007; Lefort et al., 2012). The absence of detectable porewater $\sum H_2S$ combined with a high reactive solid iron content of the sediments indicates that the precipitation of free sulfide sequesters most of the sulfide generated by SR. Nevertheless, whereas the sediments at all studied sites are iron-rich, some differences could be observed in the reactivity of the solid iron phases.

The reactivity of solid iron phases towards sulfide depends on their mineralogy (Canfield et al., 1992; Laufer et al., 2020): poorly crystalline lepidocrocite, ferrihydrite and nanoparticulate goethite are the most reactive, followed by the more crystalline hematite and goethite. Magnetite is also reactive in the presence of reduced sulfur, but over a longer

timescale (several hundreds of years) (Canfield and Berner, 1987). The reactive solid iron content of the sediment can be influenced by $[DO]_{bot}$ and sedimentation rates. Lefort et al. (2012) reported an increase in the reactive solid and dissolved iron pools after 25 years of persistent hypoxia near site H1, as more refractory phases were likely converted to reactive iron. The LSLE sediments are also rich in Fe(III) silicates (Ramachandran, 1991), and long-term exposure of less reactive Fe(III) minerals, such as crystalline oxides and silicates to sulfide, could lead to their dissolution and an increase in the reactive iron pool (Canfield et al., 1992).

Under similar $[DO]_{bot}$, OM, and detrital sources, more reactive solid iron phases will be preserved and buried at higher sedimentation rates (Liu et al., 2021; Riedinger et al., 2005, 2017). Consequently, sediments at site H1, where the sedimentation rate is highest among the studied sites, have a higher reactive solid iron content (~ + 100 µmol/g) than those at sites H2 and BR3. Additionally, there is no significant decrease in the reactive solid iron content with depth at site H1, unlike what is observed at sites BR3 and H2. It has been suggested that the availability of reactive solid iron oxides in the sediments can inhibit the conversion of AVS to pyrite (Gagnon et al., 1995; Riedinger et al., 2017). The reactivity of the iron phases may influence the rate of AVS formation and control the amount of $\sum H_2S$ that can be oxidized to intermediate valency S species (Gagnon, 1995). However, the absence of H_2S odor in the three studied cores indicates an effective scavenging of porewater sulfide by reactive solid iron phases, and the differences in reactive solid iron content suggest that AVS formation is not limited by the availability of Fe in the LSLE sediment, regardless of the site. Still, AVS accumulates to relatively high concentrations at sites BR3 and H1 (respectively (2.2 µmol·$S^{cm^{-2}}yr^{-1}$ and 3.5 µmol·$S^{cm^{-2}}yr^{-1}$) but are barely detectable at site H2 (0.2 µmol·$S^{cm^{-2}}yr^{-1}$) (Fig. 6). The re-oxidation of AVS and its conversion to pyrite seem to be the primary factors influencing the reduced S distributions in the studied cores.

1.6.1.3 Control on re-oxidation processes that affect the conversion of AVS to pyrite

The conversion of AVS to pyrite through the "polysulfide pathway" requires the reaction of AVS with sulfur species in intermediate oxidation states. These species are products of the oxidation of $\sum H_2S$ (Roberts et al., 1969; Rickard, 1975; Howarth and Jørgensen, 1984), and their abundance may decrease with distance away from the oxic/anoxic redox boundary (Gagnon et al., 1995). Alternatively, they can also be produced over time and at depth within the SR zone, by the reaction of $\sum H_2S$ and AVS with more refractory ferric minerals, such as hematite, magnetite, and silicates (Rickard and Morse, 2005). Unfortunately, we could not directly quantify AVS oxidation processes at our study sites. The role of sulfide oxidation could be estimated through additional experiments using passive or active techniques, such as measuring of the stable S isotopic composition of porewater sulfate and solid sulfides (Kaplan and Rittenberg, 1964; Mangalo et al., 2007). Voltammetric in-situ methods might also be used to identify oxidation states (Luther and Ferdelman, 1993; Luther et al., 2008). The observed discrepancies in AVS and pyrite concentrations between sites suggest that differences in re-oxidation processes play a significant role.

Variations in sedimentation rate can significantly affect the extent of re-oxidation processes by decreasing the residence time of AVS near the oxic/anoxic redox boundary (Rickard and Morse, 2005). The persistence of AVS up to 45 cm depth in an iron-rich environment with a rapid sedimentation rate has been reported in other coastal environments such as eutrophic estuarine sediments (Kraal et al., 2013), and it was proposed that pyrite formation in these sediments was inhibited by the availability of oxidants (Aller and Rude, 1988; Middelburg, 1991; Gagnon et al., 1995; Kraal et al., 2013). In our study, we observe the persistence of AVS at BR3 (9.4 μmol/g at 45 cm, Fig. 4) and H1 (6.3 μmol/g at 68 cm, Fig. 4). At site H1, AVS concentrations as high as 20.1 μmol/g are observed at 68 cm depth. Higher sedimentation rates at H1 (~ 0.4 ± 0.03 cm yr^{-1}) and BR3 (~ 0.3 ± 0.03cm yr^{-1}) than at H2 (~ 0.2 ± 0.02 cm yr^{-1}) more rapidly bury AVS and may limit its interaction with oxidants such as O_2, NO_3^- and MnO_2 that are required to generate intermediate valency S species that promote pyrite formation (Aller and Rude, 1988; Roberts et al., 1969; Rickard,

1975; Howarth and Jørgensen, 1984). In contrast, slower sedimentation rates increase the residence time of AVS near the oxic/anoxic redox boundary, as observed at H2 (Fig. 4: peak at 15 cm at H2 vs. 25/30 cm at H1), where it may be partially oxidized to intermediate oxidation state sulfur species that promote the conversion of AVS to pyrite (Gagnon et al., 1995; Chambers et al., 2000, Rickard et and Morse, 2005). At site H2, the distribution of reduced sulfur species looks like those of most coastal well-oxygenated marine systems, where the formation and persistence of AVS (<0.002 μmol/g below 25 cm at H2, Fig. 10) is limited to a thin anoxic subsurface layer below which they are converted to pyrite (Rickard and Morse 2007; Kraal et al., 2013).

The AVS content of the sediments depends on the balance between its formation and removal, either through re-oxidation or conversion into pyrite (Aller, 1977). In the presence of oxidants (e.g., oxygen, nitrate, and manganese oxides), the oxidative destruction of AVS is more rapid than the oxidative decomposition of pyrite, resulting in a small AVS-S-to-pyrite-S ratio (Aller and Rude, 1988; Schippers and Jørgensen, 2002; Rickard and Morse, 2005). Among our three study sites, site H2 was characterized by the slower sedimentation rate (Fig. 6), the lowest AVS accumulation rate, and the fastest pyrite accumulation rate (Table 4), suggesting that oxidation processes are highly dependent on sedimentation rate. As indicated earlier, the conversion of AVS into pyrite is promoted by the presence of intermediate oxidation state sulfur species, whose production is also dependent on the presence of oxidants (Berner, 1970, 1984; Rickard, 1975; Gagnon et al., 1995).

At very low $[DO]_{bot}$, the absence of bioturbating organisms would also inhibit the conversion efficiency of AVS to pyrite by limiting the depth of oxidants penetration and mixing of reduced sulfur solids to the oxic layer (Belzile and Lebel, 1986; Jørgensen and Parks, 2010). It has been determined that, in the LSLE, the bio-irrigation rate becomes negligible below a threshold $[DO]_{bot}$ of between 84 and 53 μM (Pascal et al., 2024). Although the $[DO]_{bot}$ at all the studied sites was below that threshold (Table 2), that threshold was reached more recently at site H2 than at the other two sites (Jutras et al., 2023b). X-ray tomographic scans of the cores recovered at site H1 revealed the presence of ancient burrows

filled with mud and truncated below the sediment-water interface (G. Chaillou pers. comm.; Katsev et al., 2007). In addition, the ^{210}Pb data at site H2 indicated the presence of a mixed layer in the first 5 cm of the core, a feature that was not observable in the BR3 and H1 cores. This is not conclusive evidence that bio-irrigation is still active at site H2, because $[DO]_{bot}$ is under the established threshold, but a slower sedimentation rate and reaching the threshold $[DO]_{bot}$ more recently could explain why burrows are not yet mud-filled as a relic of recent change.

1.6.2 Implication of the abundant reactive solid iron phases buffering capacity in the development of hypoxia

1.6.2.1 1.6.2.1 Abundant reactive solid iron phases in the LSLE keep the overall degree of pyritization low

The observed differences in AVS and pyrite distributions in the LSLE sediments at the three studied sites appear to arise from the differences in oxidant availability in the sediments. Our results confirm that the standing stock of reactive solid iron is sufficient to prevent $\sum H_2S$ from building up in the porewaters (Fig. 12).

Environments that are limited in iron and dominated by dissolved sulfide are called euxinic. When the overlying waters become devoid of oxygen, porewater $\sum H_2S$ can diffuse out of the sediment, increase the strength of the oxygen sink, worsen the deleterious effects of hypoxia on benthic macrofauna (Vaquer-Sunyer and Duarte, 2010) and can even lead to fish death by toxicity (Luther et al., 2004). With declining $[DO]_{bot}$ and increased production of $\sum H_2S$ in the LSLE, it is important to evaluate the buffering capacity of these iron-rich sediments. To evaluate this buffering capacity, we compared the availability of reactive solid iron oxides in sediments at our sites with those of the Bornholm Basin, a seasonally anoxic sub-basin of the Baltic Sea (Liu et al., 2021).

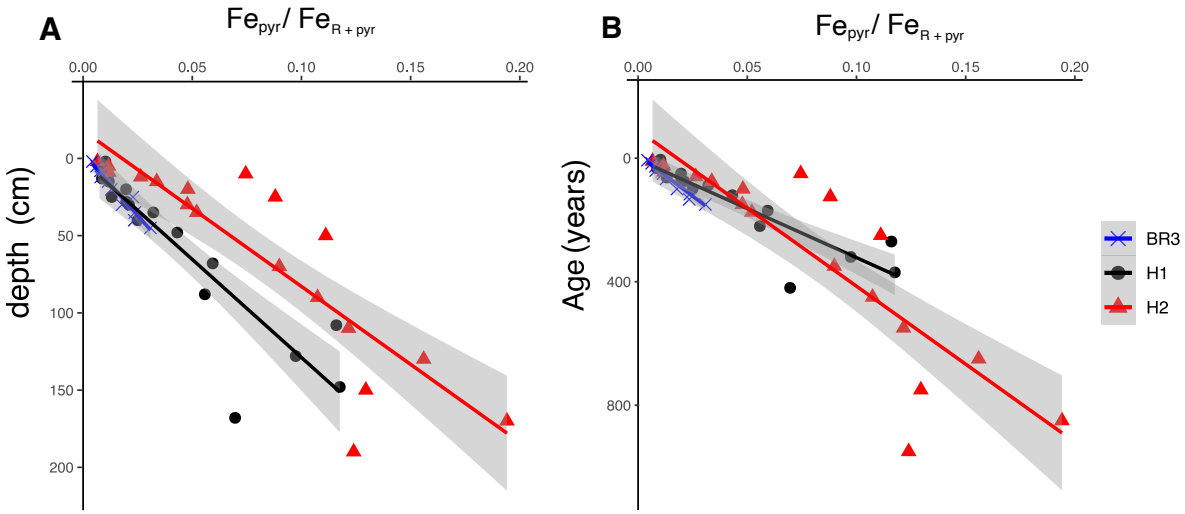

Figure 12. A) Degree of pyritization (DOP = Fepyr/(FeR+pyr)) as a function of sediment depth at sites BR3, H1 and H2 in the LSLE, with confidence intervals. B) Degree of pyritization (Fepyr/(FeR+pyr)) of sediment as a function of depositional age at sites BR3, H1 and H2 in the LSLE, with confidence intervals

All our studied sites are characterized by a low DOP (<0.2, Fig. 12; Fig. 13). When compared to the sediments of the eutrophic and intermittently anoxic Bornholm Basin (Baltic Sea) where DOP reaches values as high as 0.93 (Liu et al., 2021). The sediments of the LSLE do not appear to be limited in reactive iron and able to scavenge most if not all the $\sum H_2S$ produced by sulfate reduction, thus preventing its diffusion to the oxic/anoxic boundary where intermediate oxidation sulfur species could be generated.

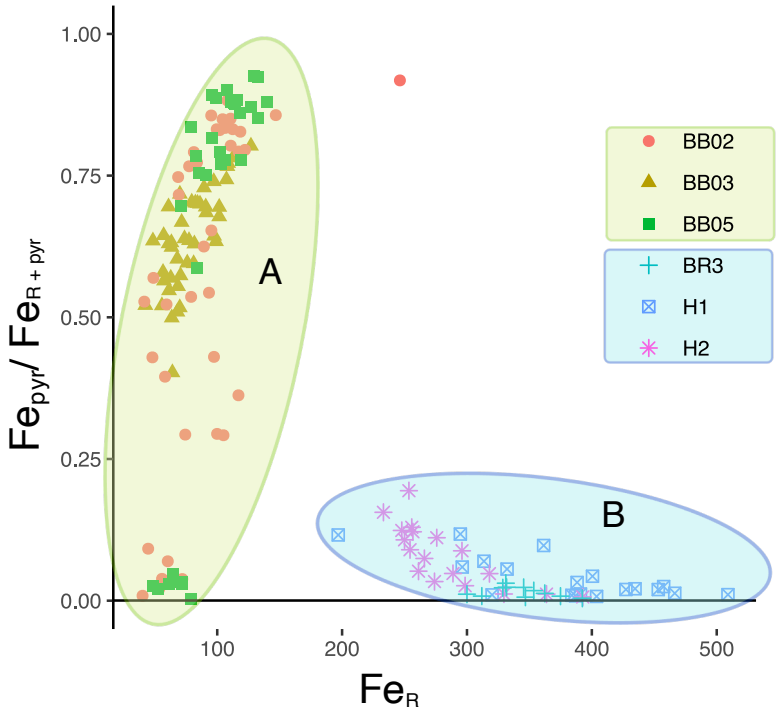

Figure 13. Degree of pyritization (DOP = $Fe_{pyr}/(Fe_{R+pyr})$) as a function of reactive solid iron concentration (Fe_R). **A**) Cluster of the sites in the eutrophic and seasonally anoxic iron-limited Bornholm Basin (Baltic Sea, (Liu et al., 2021)). **B**) Cluster of the sites in the persistently hypoxic and iron-rich sediments of the LSLE

The development of hypoxic bottom-waters in the LSLE on the sediment diagenesis is expected to increase the sulfate reduction rate and the production of reduced sulfur species $\sum H_2S$ (Katsev et al., 2007), but our findings show that the high availability of reactive iron is sufficient to sequester most of the generated $\sum H_2S$ as iron sulfides and limit its accumulation in the porewaters. Our results indicate that the LSLE, even if the $[DO]_{bot}$ decline further and anoxia develop, the abundance of reactive solid iron oxides would prevent the build up and diffusion of $\sum H_2S$ to the overlying waters. Thus, the LSLE is not likely to become an euxinic environment in a near future.

1.7 CONCLUSIONS

Near the head of the Laurentian Trough, where bottom-water hypoxia has been persistent and worsening for more than 35 years, sediment cores were recovered at three sites within a radius of ~10 km of each other. Vertical profiles showed discrepancies in the distribution of solid reduced sulfur species (AVS and pyrite) within the sediments, suggesting that the response of the sulfur cycle to persistent deoxygenation is extremely sensitive to small variations of a combination of environmental factors.

Although organic carbon exerts a major control on the S cycle by driving sulfate reduction, the small differences in organic carbon composition and content between the three sediment cores likely do not considerably impact the repartition of solid S species in the sediment. Whereas the reactive iron content of the sediment determines the locus of authigenic sulfide precipitation and limits the diffusion and, thus, the oxidation of porewater sulfides in the sediments, the abundance of reactive solid iron does not limit the formation of AVS. It does, however, inhibits the conversion of AVS to pyrite by the H2S pathway (Eq. 1) as free sulfide cannot accumulate in the LSLE sediment porewaters nor diffuse up to the oxic layer where reduced sulfur species of intermediate oxidation state could form and foster the conversion of AVS to pyrite.

The sedimentation rate exerts a major control on the diagenetic S cycle by affecting the supply of organic carbon and iron and, thus, the oxidant demand of the sediment. Furthermore, in the iron-rich sediments of the LSLE, faster sedimentation rates more rapidly distance the authigenic AVS from oxidants such as oxygen, nitrate and Mn oxides and, thus, limits the potential for the formation of polysulfides that promote the conversion of AVS to pyrite. In contrast, at lower sedimentation rates, AVS is more likely to react with oxidants and enhance its conversion into pyrite. Hence, we propose that variations of the AVS-S-to-pyrite-S ratio observed between the studied sites in the LSLE can be explained partly by the variations in their sedimentation rates.

The development of the hypoxic bottom-waters may also inhibit the conversion of AVS to pyrite by limiting bioturbation and bio-irrigation and, thus, reducing the depth of the mixed layer and the enhanced diffusion of oxygen from overlying waters, and physical mixing and exposure of solid sulfides to oxygen. As $[DO]_{bot}$ declines, the potential for AVS re-oxidation and polysulfide formation may also be diminishing. Nevertheless, the abundance of reactive iron in these sediments does not limit the authigenic precipitation of AVS and pyrite but constrains the buildup of porewater $\sum H_2S$ concentrations and, thus, its diffusion to the oxic/anoxic boundary where it could be oxidized to intermediate oxidation state sulfur species that promote the conversion of AVS to pyrite. Establishing the potential buffering capacity of reactive iron towards sulfide (Zhu et al., 2012) was important to evaluate the resilience of the ecosystem to persistent deoxygenation in the LSLE bottom-waters and the ultimate development of euxinic conditions.

1.8 CONFLICT OF INTEREST

The authors declare that the research was conducted in the absence of any commercial or financial relationships that could be construed as a potential conflict of interest.

1.9 AUTHOR CONTRIBUTION

G. Duval, A. Pellerin, G. Chaillou, and A. Mucci participated in discussions about the results and interpretations presented in this manuscript.

G. Duval wrote the first draft of all documents whereas A. Pellerin, G. Chaillou, and A. Mucci provided feedback and edited different sections of the manuscript.

G. Duval finalized the manuscript for initial submission. All authors will read and approve the version before final submission.

1.10 ACKNOWLEGMENTS

The authors thank the Réseau Québec Maritime for its financial and technical support. We also thank the captains and crews of the R/V Coriolis II for their dedicated work onboard. We thank all who participated in the field sampling and laboratory work: Camille Tran, Santiago Marquez, Ludovic Pascal, Arturo Zanon, Alexie Roy-Lafontaine, Pauline Firmin, Méliane Renaud, Silvia Zieger, Samantha Loutet and Sam McNichol. We thank Mathieu Babin and Steeven Ouelette, the ISMER-UQÀR technicians, and Jean-Carlos Montero-Serrano. We also thank the UQÀM-GEOTOP laboratories and their staff for the ^{210}Pb, $\%C_{org}$, and $\delta\,^{13}C$ analyses. This study is a contribution of the Québec-Océan and GEOTOP research networks, and it was funded by the FRQNT (Fonds de recherche du Québec – Nature et technologies) through a grant to A. Pellerin.

CONCLUSION GÉNÉRALE

Ce mémoire a permis d'étudier la distribution des espèces soufrées dans les sédiments du chenal Laurentien, entre Baie-Comeau et Rimouski, dans un contexte d'hypoxie persistante. Les principaux objectifs étaient d'établir un portrait de la répartition des espèces soufrées (sulfate, AVS et pyrite) et d'identifier les facteurs environnementaux, tels que le taux de sédimentation, la concentration en oxygène dissous des eaux profondes, la quantité et réactivité de la matière organique ainsi que la quantité de fer réactif, qui favorisent la persistance des AVS ou leur conversion en pyrite. En parallèle, cette étude visait à évaluer la capacité tampon des sédiments, associée à l' abondance en fer réactif, à limiter l'accumulation de $\sum H_2S$ dans les eaux porales.

Les analyses ont révélé une variabilité spatiale de la distribution verticale des AVS et de la pyrite entre les trois sites à l'étude malgré leur proximité géographique, soit à l'intérieur d'un rayon de 10 km. Ces résultats révèlent une sensibilité accrue du cycle du soufre à de faibles variations de facteurs environnementaux. Deux des trois sites étudiés étaient caractérisés par une importante accumulation d'AVS métastables et une faible conversion de ces AVS en pyrite, ce dernier étant un puit plus stable du soufre réduit. Ces différences se traduisaient par des ratios maximums d'AVS-S-à-pyrite-S de 0.98 et 0.85 aux deux sites situés en amont du domaine d'échantillonnage dans le LSLE et de seulement 0.18 au site situé ~20 km en aval. Ces ratios ne révélaient pas uniquement des concentrations faibles d'AVS au site en aval, mais aussi une accumulation de pyrite plus importante, atteignant 7.2 $\mu mol\ cm^{-2}\ yr^{-1}$.

Un taux d'accumulation de matière organique légèrement supérieure aux sites en amont pourrait sous-tendre des taux de sulfato-réduction légèrement supérieurs à ces sites, et donc une production plus élevée de $\sum H_2S$. Or, compte tenu de l'abondance accrue de pyrite à la station présentant les plus faibles concentrations d'AVS, une variabilité de la quantité de

$\sum H_2S$ produite par sulfato-réduction entre les sites ne suffit pas à expliquer l'ampleur des variations de la distribution verticale de ces deux principaux puits de soufre réduit. Par ailleurs, tous les sites étaient caractérisés par une grande abondance d'oxides de fer réactif solide (>200 µmol/g), ce qui atteste que la précipitation du $\sum H_2S$ n'est pas limitée par la disponibilité en fer. En résumé et pour le dire autrement, la formation d'AVS n'est pas limitée par la quantité de $\sum H_2S$ produite ni par la disponibilité d'oxides solides de fer réactif aux stations à l'étude. C'est donc la persistance des AVS qui diffère entre les sites, et l'efficacité de leur conversion en pyrite.

Malgré les faibles variations du taux de sédimentation entre les sites, ce facteur semble jouer un rôle important pour expliquer ces différences (Rickard et Morse, 2005 ; Gagnon et al., 1995). En effet, un taux de sédimentation plus lent à la station en aval permettrait une réoxydation plus efficace des AVS et du $\sum H_2S$ et la formation de polysulfures nécessaires à la formation de pyrite. Aux stations en amont, un enfouissement plus rapide des AVS inhiberait leur conversion en pyrite en les éloignant de la zone où sont présents les oxydants (oxygène, nitrates et oxides de manganèse).

La concentration en oxygène dissous dans les eaux profondes peut aussi influencer la répartition des AVS et de la pyrite dans le sédiment, en influençant la profondeur de pénétration de l'oxygène dans les sédiments. Cette profondeur conditionne la disponibilité des oxydants nécessaires à la conversion des AVS en pyrite. Par ailleurs, la désoxygénation affecte également la bioturbation en réduisant l'activité des organismes benthiques et épibenthiques, ce qui réduit l'épaisseur de la couche de mélange et limite d'avantage l'accès aux oxydants et la réoxydation des AVS. Or, la concentration en oxygène dissous des eaux profondes à tous les sites étudiés était inférieure au seuil 54 µmol/L sous lequel la bio-irrigation semble être négligeable dans l'estuaire maritime du Saint-Laurent (Pascal et al., 2024). Nos résultats indiquent que ce seuil ne suffit pas à expliquer l'efficacité de conversion de la conversion des AVS en pyrite au site en aval. Cette étude illustre l'interaction complexe entre les processus de réoxydation, la disponibilité en oxygène et les taux de sédimentation dans le contrôle de la distribution des espèces soufrées.

Le degré de pyritisation aux trois sites étudiés est inférieur à 0.2 sur les 40 premiers cm des carottes, ce qui indique que 80% du fer solide réactif demeure disponible pour la séquestration du $\sum H_2S$ produit lors de la sulfato-réduction. Ces résultats confirment que, malgré la progression de l'hypoxie dans le LSLE, la diffusion de $\sum H_2S$ toxique dans les eaux surnageantes n'est pas susceptible de se produire dans un futur proche.

Cette étude met en évidence le rôle clé des facteurs environnementaux et locaux, dont les taux de sédimentation, dans la distribution des espèces soufrées dans les sédiments du LSLE. Elle contribue également à une meilleure compréhension des impacts biogéochimiques de l'hypoxie persistante et des mécanismes de résilience des systèmes riches en fer face à la désoxygénation et pose les bases pour des études futures sur la réoxydation des espèces soufrées dans l'estuaire maritime du Saint-Laurent.

Limites et perspectives du projet

Bien que cette étude ait permis de mieux comprendre les processus de réoxydation des espèces soufrées réduites dans un système riche en fer en contexte d'hypoxie, certaines limites subsistent. L'impact spécifique de la désoxygénation sur ces processus reste difficile à cerner. Les variations des paramètres environnementaux observées entre les stations à l'étude, notamment les faibles différences des taux de sédimentation, ont complexifié l'identification de l'effet direct des variations en oxygène dissous dans les eaux profondes sur la répartition des espèces soufrés dans les sédiments. Une approche expérimentale ou l'étude des sites présentant des gradients plus marqués en oxygène dissous et taux de sédimentation pourraient permettre de mieux isoler ces variables.

Par ailleurs, des incertitudes méthodologiques subsistent concernant les mesures d'AVS. Comme l'ont souligné Rickard et Morse (2005), le processus d'extraction des AVS manque de robustesse, ce qui limite les comparaisons entre les différentes études et rend difficile le suivi temporel des concentrations. Les mesures d'AVS, sont de plus, particulièrement sensibles aux conditions d'échantillonnage et d'extraction, et leur oxydation

rapide peut conduire à des sous-estimations ou à des biais d'interprétation. Par exemple, l'analyse de carottes prélevées un an avant la mise en place de la méthode utilisée dans cette étude n'a pas pu révéler la présence d'AVS, alors que les échantillons prélevés aux mêmes sites l'année suivante avaient des concentrations significatives d'AVS. De plus, l'utilisation de réactifs tels que le chlorure d'étain lors de l'extraction séquentielle peut artificiellement augmenter les concentrations d'AVS au détriment de celles de la pyrite, ce qui a empêché une comparaison directe avec les données historiques de Gagnon et al. (1995) et Lefort et al. (2012).

Pour améliorer la compréhension des processus de réoxydation et de conversion des AVS en pyrite, des mesures complémentaires, telles que la quantification du soufre élémentaire (S(0)), des polysulfures(S_n(-II)) et l'analyse des isotopes stables du soufre des AVS, de la pyrite et des sulfates, seraient particulièrement intéressantes. Pour pouvoir tirer des conclusions sur les processus menant à la distribution des espèces soufrées, il conviendra de caractériser les réactions d'oxydo-réduction et leurs métabolites. Une attention particulière devra être portées aux phases dissoutes, puisque ce sont elles qui diffusent et peuvent réagir avec les oxydants provenant de l'interface eau-sédiment. L'utilisation de la voltampérométrie cyclique avec des microélectrodes Au/Hg pourrait permettre de mesurer simultanément les principales espèces redox impliquées dans la diagenèse précoce (O_2, Mn^{2+}, Fe^{2+}, HS^-, FeS et Fe(III)) (Luther et Ferdelman, 1993 ; Luther et al., 2008). Ces approches pourraient fournir de précieuses informations sur les voies spécifiques de réoxydation et leur importance relative dans le système étudié. Finalement, le but de ce mémoire, qui visait à dresser un portait des espèces soufrées dans les sédiments du LSLE, est atteint. Pour filer la métaphore, il s'agissait d'une analyse d'un tableau déjà sec. Pour mieux comprendre les processus en jeu, il faudra ensuite observer comment la peinture fraîche se dépose et se mélange sur la toile sous-marine des sédiments du chenal laurentien.

RÉFÉRENCES BIBLIOGRAPHIQUES

Alkhatib, M., Schubert, C. J., del Giorgio, P. A., Gélinas, Y., and Lehmann, M. F. (2012). Organic matter reactivity indicators in sediments of the St. Lawrence Estuary. *Estuarine, coastal and shelf science*, *102-103*, 36-47.

Aller, R. C. (1977). *Influence of macrobenthos on chemical diagenesis of marine sediments* [Thèse de doctorat]. https://doi.org/10.2172/7218600

Aller, R. C. (1994). Bioturbation and remineralization of sedimentary organic matter : Effects of redox oscillation. *Chemical Geology*, *114*(3), 331-345. https://doi.org/10.1016/0009-2541(94)90062-0

Aller, R. C., and Rude, P. D. (1988). Complete oxidation of solid phase sulfides by manganese and bacteria in anoxic marine sediments. *Geochimica et Cosmochimica Acta*, *52*(3), 751-765. https://doi.org/10.1016/0016-7037(88)90335-3

Aquino-López, M., Blaauw, M., Christen, J., and Sanderson, N. (2018). Bayesian Analysis of 210Pb Dating. *Journal of Agricultural, Biological and Environmental Statistics*, *23*. https://doi.org/10.1007/s13253-018-0328-7

Audet, T., de Vernal, A., Mucci, A., Seidenkrantz, M.-S., Hillaire-Marcel, C., Carnero-Bravo, V., and Gélinas, Y. (2023). Benthic Foraminiferal Assemblages from the Laurentian Channel in the Lower Estuary and Gulf of ST. Lawrence, Eastern Canada : Tracers of Bottom-Water Hypoxia. *Journal of Foraminiferal Research*, *53*(1), 57-77. https://doi.org/10.2113/gsjfr.53.1.57

Bauer, J. E., Cai, W.-J., Raymond, P. A., Bianchi, T. S., Hopkinson, C. S., and Regnier, P. A. G. (2013). The changing carbon cycle of the coastal ocean. *Nature*, *504*(7478), 61-70. https://doi.org/10.1038/nature12857

Beam, J. P., Michaud, A. B., Johnston, D. T., Girguis, P. R., and Emerson, D. (2022). Impacts of bioturbation on iron biogeochemistry and microbial communities in coastal sediment mesocosms under varying degrees of hypoxia. *Estuarine, Coastal and Shelf Science*, *276*, 108032.

Belzile, M., Galbraith, P. S., and Bourgault, D. (2016). Water renewals in the Saguenay Fjord. *Journal of Geophysical Research: Oceans*, *121*(1), 638-657. https://doi.org/10.1002/2015JC011085

Belzile, N., and Lebel, J. (1986). Capture of arsenic by pyrite in near-shore marine sediments. *Chemical Geology*, *54*(3-4), 279-281.

Berner, R. (1980). *Early diagenesis : A theoretical approach* (Vol. 241). Princeton University Press.

Berner, R. A. (1964). Distribution and diagenesis of sulfur in some sediments from the Gulf of California. *Marine Geology*, *1*(2), 117-140.

Berner, R. A. (1970). Sedimentary pyrite formation. *American Journal of Science*, *268*(1), 1-23.

Berner, R. A. (1978). Sulfate reduction and the rate of deposition of marine sediments. *Earth and Planetary Science Letters*, *37*(3), 492-498. https://doi.org/10.1016/0012-821X(78)90065-1

Berner, R. A. (1984). Sedimentary pyrite formation : An update. *Geochimica et Cosmochimica Acta*, *48*(4), 605-615. https://doi.org/10.1016/0016-7037(84)90089-9

Berner, R. A., De Leeuw, J. W., Spiro, B., Murchison, D. G., Eglinton, G., Eglinton, G., Curtis, C. D., McKenzie, D. P., and Murchison, D. G. (1997). Sulphate reduction, organic matter decomposition and pyrite formation. *Philosophical Transactions of the Royal Society of London. Series A, Mathematical and Physical Sciences*, *315*(1531), 25-38. https://doi.org/10.1098/rsta.1985.0027

Boesen, C., and Postma, D. (1988). Pyrite formation in anoxic environments of the Baltic. *American Journal of Science*, *288*(6), 575-603.

Boulegue, J. (1976). Equilibres dans filesysteme H2S–S8 colloıde-H2O. *Comptes Rendus Acad. Sci. Paris D*, *283*, 591-594.

Breitburg, D., Levin, L. A., Oschlies, A., Grégoire, M., Chavez, F. P., Conley, D. J., Garçon, V., Gilbert, D., Gutiérrez, D., Isensee, K., Jacinto, G. S., Limburg, K. E., Montes, I., Naqvi, S. W. A., Pitcher, G. C., Rabalais, N. N., Roman, M. R., Rose, K. A., Seibel, B. A. and Zhang, J. (2018). Declining oxygen in the global ocean and coastal waters. *Science (New York, N.Y.)*, *359*(6371), https://doi.org/10.1126/science.aam7240

Bugden, G. L. (1991). Changes in the temperature-salinity characteristics of the deeper waters of the Gulf of St. Lawrence over the past several decades. *The Gulf of St. Lawrence: Small Ocean or Big Estuary, Can. Sp. Pub. Fish. Aquat. Sci.*, *113*, 139-147.

Burdige, D. J. (2007). Preservation of organic matter in marine sediments : Controls, mechanisms, and an imbalance in sediment organic carbon budgets? *Chemical Reviews*, *107*(2), 467-485.

Butler, I. B., Böttcher, M. E., Rickard, D., and Oldroyd, A. (2004). Sulfur isotope partitioning during experimental formation of pyrite via the polysulfide and hydrogen sulfide pathways : Implications for the interpretation of sedimentary and hydrothermal pyrite isotope records. *Earth and Planetary Science Letters*, *228*(3), 495-509. https://doi.org/10.1016/j.epsl.2004.10.005

Canfield, D. E., and Berner, R. A. (1987). Dissolution and pyritization of magnetite in anoxie marine sediments. *Geochimica et Cosmochimica Acta*, *51*(3), 645-659.

Canfield, D. E., Boudreau, B. P., Mucci, A., and Gundersen, J. K. (1998). The Early Diagenetic Formation of Organic Sulfur in the Sediments of Mangrove Lake, Bermuda. *Geochimica et Cosmochimica Acta*, *62*, 767-781. https://doi.org/10.1016/S0016-7037(98)00032-5

Canfield, D. E., Raiswell, R., Westrich, J. T., Reaves, C. M., and Berner, R. A. (1986). The use of chromium reduction in the analysis of reduced inorganic sulfur in sediments and shales. *Chemical Geology*, *54*(1), 149-155. https://doi.org/10.1016/0009-2541(86)90078-1

Canfield, D., Raiswell, R., and Bottrell, S. H. (1992). The reactivity of sedimentary iron minerals toward sulfide. *American Journal of Science*, *292*. https://doi.org/10.2475/ajs.292.9.659

Casse, M., Montero-Serrano, J.-C., and St-Onge, G. (2017). Influence of the Laurentide Ice Sheet and relative sea-level changes on sediment dynamics in the Estuary and Gulf of St. Lawrence since the last deglaciation. *Boreas*, *46*(3), 541-561. https://doi.org/10.1111/bor.12230

Chambers, R. M., Hollibaugh, J. T., Snively, C. S., and Plant, J. N. (2000). Iron, Sulfur, and Carbon Diagenesis in Sediments of Tomales Bay, California. *Estuaries*, *23*(1), 1-9. JSTOR. https://doi.org/10.2307/1353220

Chen, K. Y., and Gupta, S. K. (1973). Formation of polysulfides in aqueous solution. *Environmental Letters*, *4*(3), 187-200.

Cline, J. D. (1969). Spectrophotometric determination of hydrogen sulfide in natural waters 1. *Limnology and Oceanography*, *14*(3), 454-458.

Conley, D. J., Carstensen, J., Ærtebjerg, G., Christensen, P. B., Dalsgaard, T., Hansen, J. L. S., and Josefson, A. B. (2007). Long-Term Changes and Impacts of Hypoxia in Danish Coastal Waters. *Ecological Applications*, *17*(5), S165-S184. JSTOR.

Cool, J., Chaillou, G., and Mucci, A. (2022). *Étude de la dynamique de l'oxygène dans les sédiments du chenal laurentien* [Mémoire de maîtrise]. Université du Québec à Rimouski.

Cornwell, J. C., and Morse, J. W. (1987). The characterization of iron sulfide minerals in anoxic marine sediments. *IX International Symposium on the Chemistry of the Mediterranean*, *22*(2), 193-206. https://doi.org/10.1016/0304-4203(87)90008-9

Diaz, R. J. (2001). Overview of Hypoxia around the World. *Journal of Environmental Quality*, *30*(2), 275-281. https://doi.org/10.2134/jeq2001.302275x

Diaz, R. J., and Rosenberg, R. (1995). Marine benthic hypoxia : A review of its ecological effects and the behavioural responses of benthic macrofauna. *Oceanography and Marine Biology. An Annual Review*, *33*(245), 03.

Diaz, R. J., and Rosenberg, R. (2008). Spreading dead zones and consequences for marine ecosystems. *Science*, *321*(5891), 926-929. https://doi.org/10.1126/science.1156401

Dickie L. M. and Trites R. W. (1983). The Gulf of St. Lawrence. *Estuaries and Enclosed Seas*, *26*, 403-425.

Drinkwater, K., and Gilbert, D. (2004). Hydrographic variability in the waters of the Gulf of St. Lawrence, the Scotian Shelf and the eastern Gulf of Maine (NAFO Subarea 4) during 1991-2000. *Journal of Northwest Atlantic Fishery Science*, *34*.

Duan, L., Song, J., Yin, M., Yuan, H., Li, X., Zhang, Y., and Yin, X. (2021). Dynamics of arsenic and its interaction with Fe and S at the sediment-water interface of the seasonal hypoxic Changjiang Estuary. *Science of The Total Environment*, *769*, 145269. https://doi.org/10.1016/j.scitotenv.2021.145269

Edenborn, H. M., Silverberg, N., Mucci, A., and Sundby, B. (1987). Sulfate reduction in deep coastal marine sediments. *Marine Chemistry*, *21*(4), 329-345.

El-Sabh, M. I., and Silverberg, N. (1990). The St. Lawrence Estuary : Introduction. Dans *Oceanography of a Large-Scale Estuarine system* (p. 1-9). Springer.

Falkowski, P. G., Algeo, T., Codispoti, L., Deutsch, C., Emerson, S., Hales, B., Huey, R. B., Jenkins, W. J., Kump, L. R., and Levin, L. A. (2011). Ocean deoxygenation : Past, present, and future. *Eos, Transactions American Geophysical Union*, *92*(46), 409-410.

Flynn, W. W. (1968). The determination of low levels of polonium-210 in environmental materials. *Analytica Chimica Acta*, *43*, 221-227. https://doi.org/10.1016/S0003-2670(00)89210-7

Fossing, H., and Jørgensen, B. B. (1989). Measurement of bacterial sulfate reduction in sediments : Evaluation of a single-step chromium reduction method. *Biogeochemistry*, *8*(3), 205-222. https://doi.org/10.1007/BF00002889

Fredriksson, J. P., Attard, K., Stranne, C., Koszalka, I. M., Glud, R. N., Andersen, T. J., Humborg, C., and Brüchert, V. (2024). Hidden seafloor hypoxia in coastal waters. *Limnology and Oceanography*, *69, 2489-250*. https://doi.org/10.1002/lno.12607

Froelich, P., Klinkhammer, G., Bender, M. L., Luedtke, N., Heath, G. R., Cullen, D., Dauphin, P., Hammond, D., Hartman, B., and Maynard, V. (1979). Early oxidation of organic matter in pelagic sediments of the eastern equatorial Atlantic : Suboxic diagenesis. *Geochimica et Cosmochimica Acta*, *43*(7), 1075-1090.

Gagnon, C., Mucci, A., and Pelletier, É. (1995). Anomalous accumulation of acid-volatile sulphides (AVS) in a coastal marine sediment, Saguenay Fjord, Canada. *Geochimica et Cosmochimica Acta*, *59*(13), 2663-2675. https://doi.org/10.1016/0016-7037(95)00163-T

Gagnon, C., Mucci, A., and Pelletier, E. (1996). Anomalous accumulation of acid-volatile sulphides (AVS) in a coastal marine sediment, Saguenay Fjord, Canada. *Oceanographic Literature Review*, *1*(43), 33.

Genovesi, L., De Vernal, A., Thibodeau, B., Hillaire-Marcel, C., Mucci, A., and Gilbert, D. (2011). Recent changes in bottom water oxygenation and temperature in the Gulf of St. Lawrence : Micropaleontological and geochemical evidence. *Limnology and Oceanography*, *56*(4), 1319-1329.

Gilbert, D., Sundby, B., Gobeil, C., Mucci, A., and Tremblay, G. (2005). A seventy-two-year record of diminishing deep-water oxygen in the St. Lawrence estuary : The northwest Atlantic connection. *Limnology and Oceanography*, *50*(5), 1654-1666.

Gobeil, C. (2006). Biogeochemistry and Chemical Contamination in the St. Lawrence Estuary. Dans P. J. Wangersky (Éd.), *Estuaries* (p. 121-147). Springer Berlin Heidelberg. https://doi.org/10.1007/698_5_023

Goldhaber, M., and Kaplan, I. (1974). The sulfur cycle. *The Sea. John Wiley and Sons, New York, New York, USA*, 569-655.

Gooday, A., Jorissen, F., Levin, L., Middelburg, J., Naqvi, S., Rabalais, N., Scranton, M., and Zhang, J. (2009). Historical records of coastal eutrophication-induced hypoxia. *Biogeosciences*, *6*(8), 1707-1745.

Grasshoff, K., Kremling, K., and Ehrhardt, M. (2009). *Methods of Seawater Analysis*. John Wiley and Sons.

Howarth, R., Chan, F., Conley, D. J., Garnier, J., Doney, S. C., Marino, R., and Billen, G. (2011). Coupled biogeochemical cycles : Eutrophication and hypoxia in temperate estuaries and coastal marine ecosystems. *Frontiers in Ecology and the Environment*, *9*(1), 18-26. https://doi.org/10.1890/100008

Howarth, R. W., and Jørgensen, B. B. (1984). Formation of 35S-labelled elemental sulfur and pyrite in coastal marine sediments (Limfjorden and Kysing Fjord, Denmark) during short-term 35SO42− reduction measurements. *Geochimica et Cosmochimica acta*, *48*(9), 1807-1818.

Jaegle, M. (2015). *Nature et origine des sédiments de surface de l'estuaire du Saint-Laurent*. Université du Québec à Rimouski.

Jessen, G. L., Lichtschlag, A., Ramette, A., Pantoja, S., Rossel, P. E., Schubert, C. J., Struck, U., and Boetius, A. (2017). Hypoxia causes preservation of labile organic matter and changes seafloor microbial community composition (Black Sea). *Science Advances*, *3*(2), e1601897. https://doi.org/10.1126/sciadv.1601897

Jørgensen, B. (2006). Bacteria and Marine Biogeochemistry. Dans *Marine Geochemistry* (p. 169-206). https://doi.org/10.1007/3-540-32144-6_5

Jørgensen, B. B. (1977). The sulfur cycle of a coastal marine sediment (Limfjorden, Denmark) 1. *Limnology and Oceanography*, *22*(5), 814-832.

Jørgensen, B. B. (1982). Mineralization of organic matter in the sea bed—The role of sulphate reduction. *Nature*, *296*(5858), 643-645.

Jørgensen, B. B. (1990). A thiosulfate shunt in the sulfur cycle of marine sediments. *Science*, *249*(4965), 152-154.

Jørgensen, B. B., Findlay, A. J., and Pellerin, A. (2019). The Biogeochemical Sulfur Cycle of Marine Sediments. *Frontiers in Microbiology*, *10*. https://doi.org/10.3389/fmicb.2019.00849

Jørgensen, B. B., and Parkes, R. J. (2010). Role of sulfate reduction and methane production by organic carbon degradation in eutrophic fjord sediments (Limfjorden, Denmark). *Limnology and Oceanography*, *55*(3), 1338-1352. https://doi.org/10.4319/lo.2010.55.3.1338

Jutras, M., Dufour, C. O., Mucci, A., Cyr, F., and Gilbert, D. (2020). Temporal Changes in the Causes of the Observed Oxygen Decline in the St. Lawrence Estuary. *Journal of Geophysical Research: Oceans*, *125*(12), e2020JC016577. https://doi.org/10.1029/2020JC016577

Jutras, M., Dufour, C. O., Mucci, A., and Talbot, L. C. (2023). Large-scale control of the retroflection of the Labrador Current. *Nature Communications*, *14*(1), 2623. https://doi.org/10.1038/s41467-023-38321-y

Jutras, M., Mucci, A., Chaillou, G., Nesbitt, W. A., and Wallace, D. W. R. (2023). Temporal and spatial evolution of bottom-water hypoxia in the St Lawrence estuarine system. *Biogeosciences*, *20*(4), 839-849. https://doi.org/10.5194/bg-20-839-2023

Kafantaris, F.-C. A., and Druschel, G. K. (2020). Kinetics of the nucleophilic dissolution of hydrophobic and hydrophilic elemental sulfur sols by sulfide. *Geochimica et Cosmochimica Acta*, *269*, 554-565. https://doi.org/10.1016/j.gca.2019.11.010

Kamyshny, A., Druschel, G., Mansaray, Z. F., and Farquhar, J. (2014). Multiple sulfur isotopes fractionations associated with abiotic sulfur transformations in Yellowstone National Park geothermal springs. *Geochemical Transactions*, *15*, 1-22.

Kamyshny, A., Goifman, A., Gun, J., Rizkov, D., and Lev, O. (2004). Equilibrium distribution of polysulfide ions in aqueous solutions at 25 C: a new approach for the study of polysulfides' equilibria. *Environmental Science and Technology*, *38*(24), 6633-6644.

Kaplan, I. R., and Rittenberg, S. C. (1964). Microbiological fractionation of sulphur isotopes. *Microbiology (Reading, England)* *34*(2), 195-212. https://doi.org/10.1099/00221287-34-2-195

Katsev, S., Chaillou, G., Sundby, B., and Mucci, A. (2007). Effects of progressive oxygen depletion on sediment diagenesis and fluxes : A model for the lower St. Lawrence River Estuary. *Limnology and Oceanography*, *52*(6), 2555-2568. https://doi.org/10.4319/lo.2007.52.6.2555

Keeling, R. F., Körtzinger, A., and Gruber, N. (2010). Ocean deoxygenation in a warming world. *Annual Review of Marine Science*, *2*(1), 199-229.

Kennett, J. P., and Ingram, B. L. (1995). A 20,000-year record of ocean circulation and climate change from the Santa Barbara basin. *Nature*, *377*(6549), 510-514.

King, L. H., and MacLean, B. (1970). Origin of the outer part of the Laurentian Channel. *Canadian Journal of Earth Sciences*, *7*(6), 1470-1484.

Kraal, P., Burton, E. D., and Bush, R. T. (2013). Iron monosulfide accumulation and pyrite formation in eutrophic estuarine sediments. *Geochimica et Cosmochimica Acta*, *122*, 75-88. https://doi.org/10.1016/j.gca.2013.08.013

Kristiansen, K. D., Kristensen, E., and Jensen, E. M. H. (2002). The Influence of Water Column Hypoxia on the Behaviour of Manganese and Iron in Sandy Coastal Marine Sediment. *Estuarine, Coastal and Shelf Science*, *55*(4), 645-654. https://doi.org/10.1006/ecss.2001.0934

Laufer, K., Michaud, A. B., Røy, H., and Jørgensen, B. B. (2020). Reactivity of Iron Minerals in the Seabed Toward Microbial Reduction – A Comparison of Different Extraction Techniques. *Geomicrobiology Journal*, *37*(2), 170-189. https://doi.org/10.1080/01490451.2019.1679291

Lefort, S., Mucci, A., and Sundby, B. (2012). Sediment Response to 25 Years of Persistent Hypoxia. *Aquatic Geochemistry*, *18*(6), 461-474. https://doi.org/10.1007/s10498-012-9173-4

Liu, J., Pellerin, A., Antler, G., Kasten, S., Findlay, A. J., Dohrmann, I., Røy, H., Turchyn, A. V., and Jørgensen, B. B. (2020). Early diagenesis of iron and sulfur in Bornholm Basin sediments : The role of near-surface pyrite formation. *Geochimica et Cosmochimica Acta*, *284*, 43-60. https://doi.org/10.1016/j.gca.2020.06.003

Loring, D. H., and Nota, D. J. G. (1968). Occurrence and significance of iron, manganese, and titanium in glacial marine sediments from the Estuary of the St. Lawrence River. *Journal of the Fisheries Board of Canada*, *25*(11), 2327-2347.

Loring, D. H., and Nota, D. J. G. (1973). *Morphology and sediments of the Gulf of St. Lawrence*. Fisheries Research Board of Canada Bulletin 182, 147 p.

Lucotte, M., Hillaire-Marcel, C., and Louchouarn, P. (1991). First-order organic carbon budget in the St Lawrence Lower estuary from 13C data. *Estuarine, Coastal and Shelf Science*, *32*(3), 297-312. https://doi.org/10.1016/0272-7714(91)90022-4

Luther, G. W., Glazer, B. T., Ma, S., Trouwborst, R. E., Moore, T. S., Metzger, E., Kraiya, C., Waite, T. J., Druschel, G., Sundby, B., Taillefert, M., Nuzzio, D. B., Shank, T. M., Lewis, B. L., and Brendel, P. J. (2008). Use of voltammetric solid-state (micro)electrodes for studying biogeochemical processes : Laboratory measurements to real time measurements with an in situ electrochemical analyzer (ISEA). *Marine Chemistry*, *108*(3), 221-235. https://doi.org/10.1016/j.marchem.2007.03.002

Luther, G. W. I., and Ferdelman, T. G. (1993). Voltammetric characterization of iron(II) sulfide complexes in laboratory solutions and in marine waters and porewaters. *Environmental Science and Technology*, *27*(6), 1154-1163. https://doi.org/10.1021/es00043a015

Luther, G. W., Ma, S., Trouwborst, R., Glazer, B., Blickley, M., Scarborough, R. W., and Mensinger, M. G. (2004). The roles of anoxia, H2S, and storm events in fish kills of dead-end canals of Delaware inland bays. *Estuaries*, *27*(3), 551-560. https://doi.org/10.1007/BF02803546

Luther III, G. W. (1991). Pyrite synthesis via polysulfide compounds. *Geochimica et Cosmochimica Acta*, *55*(10), 2839-2849.

Lyons, T. W. (1997). Sulfur isotopic trends and pathways of iron sulfide formation in upper Holocene sediments of the anoxic Black Sea. *Geochimica et Cosmochimica Acta*, *61*(16), 3367-3382. https://doi.org/10.1016/S0016-7037(97)00174-9

Mangalo, M., Meckenstock, R. U., Stichler, W., and Einsiedl, F. (2007). Stable isotope fractionation during bacterial sulfate reduction is controlled by reoxidation of intermediates. *Geochimica et Cosmochimica Acta*, *71*(17), 4161-4171. https://doi.org/10.1016/j.gca.2007.06.058

Middelburg, J. J. (1991). Organic carbon, sulphur, and iron in recent semi-euxinic sediments of Kau Bay, Indonesia. *Geochimica et Cosmochimica Acta*, *55*(3), 815-828. https://doi.org/10.1016/0016-7037(91)90344-5

Middelburg, J. J. (2019). *Marine Carbon Biogeochemistry : A Primer for Earth System Scientists*. Springer Nature.

Middelburg, J. J., and Levin, L. A. (2009). Coastal hypoxia and sediment biogeochemistry. *Biogeosciences*, *6*(7), 1273-1293. https://doi.org/10.5194/bg-6-1273-2009

Oenema, O. (1990). Sulfate reduction in fine-grained sediments in the Eastern Scheldt, southwest Netherlands. *Biogeochemistry*, *9*(1), 53-74. https://doi.org/10.1007/BF00002717

Park, Y., Cha, J., Song, B., Huang, Y., Kim, S., Kim, S., Jo, E., Fortin, S., and An, S. (2020). Total Microbial Activity and Sulfur Cycling Microbe Changes in Response to the Development of Hypoxia in a Shallow Estuary. *Ocean Science Journal*, *55*(1), 165-181. https://doi.org/10.1007/s12601-020-0011-0

Pascal, L., Cool, J., Archambault, P., Calosi, P., Cuenca, A. L. R., Mucci, A. O., and Chaillou, G. (2024). Ocean deoxygenation caused non-linear responses in the structure and functioning of benthic ecosystems. *Global Change Biology*, *30*(1), e16994. https://doi.org/10.1111/gcb.16994

Peeters, F., Kipfer, R., Achermann, D., Hofer, M., Aeschbach-Hertig, W., Beyerle, U., Imboden, D. M., Rozanski, K., and Fröhlich, K. (2000). Analysis of deep-water exchange in the Caspian Sea based on environmental tracers. *Deep Sea Research Part I: Oceanographic Research Papers*, *47*(4), 621-654. https://doi.org/10.1016/S0967-0637(99)00066-7

Poulton, S. W., and Canfield, D. E. (2005). Development of a sequential extraction procedure for iron : Implications for iron partitioning in continentally derived particulates. *Chemical Geology*, *214*(3), 209-221. https://doi.org/10.1016/j.chemgeo.2004.09.003

Poulton, S. W., and Raiswell, R. (2005). Chemical and physical characteristics of iron oxides in riverine and glacial meltwater sediments. *Chemical Geology*, *218*(3-4), 203-221.

R Core Team. (2022). *R: A Language and Environment for statistical Computing* (Version 4.2.1) [Software]. R foundation for Statistical Computing. https://www.R-project.org/

Rabalais, N., Díaz, R., Levin, L., Turner, R., Gilbert, D., and Zhang, J. (2009). Dynamics and distribution of natural and human-caused coastal hypoxia. *Biogeosciences Discussions*, *6*(5).

Rabouille, C., Lansard, B., Owings, S. M., Rabalais, N. N., Bombled, B., Metzger, E., Richirt, J., Eitel, E. M., Boever, A. D., Beckler, J. S., and Taillefert, M. (2021). Early diagenesis in the hypoxic and acidified zone of the northern gulf of mexico : Is organic matter recycling in sediments disconnected from the water column? *Frontiers in Marine Science*, *8*. https://doi.org/10.3389/fmars.2021.604330

Raiswell, R., and Berner, R. A. (1985). Pyrite formation in euxinic and semi-euxinic sediments. *American Journal of Science*, *285*(8), 710-724.

Raiswell, R., Buckley, F., Berner, R. A., and Anderson, T. F. (1988). Degree of pyritization of iron as a paleoenvironmental indicator of bottom-water oxygenation. *Journal of Sedimentary Research*, *58*(5), 812-819. https://doi.org/10.1306/212F8E72-2B24-11D7-8648000102C1865D

Raiswell, R., and Canfield, D. (2012). The Iron Biogeochemical Cycle Past and Present. *Geochemical Perspectives*, *1*, 1-220. https://doi.org/10.7185/geochempersp.1.1

Raiswell, R., Canfield, D. E., and Berner, R. A. (1994). A comparison of iron extraction methods for the determination of degree of pyritisation and the recognition of iron-limited pyrite formation. *Chemical Geology*, *111*(1), 101-110. https://doi.org/10.1016/0009-2541(94)90084-1

Ramachandran, R. (1991). *Geochemical and mineralogical characteristics of some fine post-glacial marine deposits in the St. Lawrence Lowlands*. McGill University (Canada).

Regnier, P., Resplandy, L., Najjar, R. G., and Ciais, P. (2022). The land-to-ocean loops of the global carbon cycle. *Nature*, *603*(7901), 401-410. https://doi.org/10.1038/s41586-021-04339-9

Rickard, D., and Luther, G. W. (2007). Chemistry of iron sulfides. *Chemical Reviews*, *107*(2), 514-562.

Rickard, D., and Morse, J. W. (2005). Acid volatile sulfide (AVS). *Marine Chemistry*, *97*(3), 141-197. https://doi.org/10.1016/j.marchem.2005.08.004

Rickard, D., Oldroyd, A., and Cramp, A. (1999). Voltammetric evidence for soluble FeS complexes in anoxic estuarine muds. *Estuaries*, *22*(3), 693-701. https://doi.org/10.2307/1353056

Rickard, D. T. (1975). Kinetics and mechanism of pyrite formation at low temperatures. *American Journal of Science*, *275*(6), 636-652.

Riedinger, N. (2005). *Preservation and Diagenetic Overprint of Geochemical and Geophysical Signals in Ocean Margin Sediments Related to Depositional Dynamics*. Berichte, 242, Fachbereich Geowissenschaften, Universität Bremen, 91.

Riedinger, N., Brunner, B., Krastel, S., Arnold, G. L., Wehrmann, L. M., Formolo, M. J., Beck, A., Bates, S. M., Henkel, S., Kasten, S., and Lyons, T. W. (2017). Sulfur Cycling in an Iron Oxide-Dominated, Dynamic Marine Depositional System : The Argentine Continental Margin. *Frontiers in Earth Science*, *5*. https://www.frontiersin.org/journals/earth-science/articles/10.3389/feart.2017.00033

Roberts, W. M. B., Walker, A. L., and Buchanan, A. S. (1969). The chemistry of pyrite formation in aqueous solution and its relation to the depositional environment. *Mineralium Deposita*, *4*(1), 18-29. https://doi.org/10.1007/BF00206645

Schippers, A., and Jørgensen, B. (2002). Biogeochemistry of pyrite and iron sulfide oxidation in marine sediments. *Geochimica et Cosmochimica Acta*, *66*, 85-92. https://doi.org/10.1016/S0016-7037(01)00745-1

Silverberg, N. (1978). Sediments of the Rimouski shelf region, lower Saint Lawrence estuary. *Canadian Journal of Earth Sciences*, *15*(11), 1724-1736. https://doi.org/10.1139/e78-182

Smith, J. N., and Schafer, C. T. (1999). Sedimentation, bioturbation, and Hg uptake in the sediments of the estuary and Gulf of St. Lawrence. *Limnology and Oceanography*, *44*(1), 207-219. https://doi.org/10.4319/lo.1999.44.1.0207

Soetaert, K., Middelburg, J., Herman, P., and Buis, K. (2000). On the coupling of benthic and pelagic biogeochemical models. *Earth-Science Reviews*, *51*, 173-201. https://doi.org/10.1016/S0012-8252(00)00004-0

Steudel, R. (2003). Inorganic polysulfides S n 2− and radical anions S n·−. *Elemental Sulfur and Sulfur-Rich Compounds II*, 127-152.

Stevens, S. W., Pawlowicz, R., Tanhua, T., Gerke, L., Nesbitt, W. A., Drozdowski, A., Chassé, J., and Wallace, D. W. (2024). Deep inflow transport and dispersion in the Gulf of St. Lawrence revealed by a tracer release experiment. *Communications Earth and Environment*, *5*(1), 338.

Stoicescu, S.-T., Hoikkala, L., Fleming, V., and Lips, U. (2024). Continuing long-term expansion of low-oxygen conditions in the Eastern Gulf of Finland. *Oceanologia*, *66*(1), 139-152. https://doi.org/10.1016/j.oceano.2024.02.002

Stookey, L. L. (1970). Ferrozine-a new spectrophotometric reagent for iron. *Analytical Chemistry*, *42*(7), 779-781. https://doi.org/10.1021/ac60289a016

Sturdivant, S. K., Díaz, R. J., and Cutter, G. R. (2012). Bioturbation in a Declining Oxygen Environment, in situ Observations from Wormcam. *PLOS ONE*, *7*(4), e34539. https://doi.org/10.1371/journal.pone.0034539

Sundby, B. (2006). Transient state diagenesis in continental margin muds. *Marine Chemistry*, *102*(1-2), 2-12.

Sundby, B., Martinez, P., and Gobeil, C. (2004). Comparative geochemistry of cadmium, rhenium, uranium, and molybdenum in continental margin sediments. *Geochimica et Cosmochimica Acta*, *68*(11), 2485-2493. https://doi.org/10.1016/j.gca.2003.08.011

Thibodeau, B., de Vernal, A., and Mucci, A. (2006). Recent eutrophication and consequent hypoxia in the bottom waters of the Lower St. Lawrence Estuary : Micropaleontological and geochemical evidence. *Marine Geology*, *231*(1), 37-50. https://doi.org/10.1016/j.margeo.2006.05.010

Thode-Andersen, S., and Jørgensen, B. (1989). Sulfate reduction and the formation of 35S-labeled FeS, FeS2, and S0 in coastal marine sediments. *Limnology and Oceanography - LIMNOL OCEANOGR*, *34*, 793-806. https://doi.org/10.4319/lo.1989.34.5.0793

Toth, D., and Lerman, A. (1977). Organic matter reactivity and sedimentation rates in the ocean. *American Journal of Science*, *277*(4), 465-485.

Vairavamurthy, M. A., Orr, W. L., and Manowitz, B. (1995). *Geochemical Transformations of Sedimentary Sulfur : An Introduction*. ACS Publications.

van der Zee, C., Roberts, D. R., Rancourt, D. G., and Slomp, C. P. (2003). Nanogoethite is the dominant reactive oxyhydroxide phase in lake and marine sediments. *Geology*, *31*(11), 993-996.

Vaquer-Sunyer, R., and Duarte, C. M. (2010). Sulfide exposure accelerates hypoxia-driven mortalit. *Limnology and Oceanography*, *55*(3), 1075-1082. https://doi.org/10.4319/lo.2010.55.3.1075

Whitney, M. M., and Vlahos, P. (2021). Reducing Hypoxia in an Urban Estuary Despite Climate Warming. *Environmental Science and Technology*, *55*(2), 941-951. https://doi.org/10.1021/acs.est.0c03964

Zhang, J., Gilbert, D., Gooday, A. J., Levin, L., Naqvi, S. W. A., Middelburg, J. J., Scranton, M., Ekau, W., Peña, A., Dewitte, B., Oguz, T., Monteiro, P. M. S., Urban, E., Rabalais, N. N., Ittekkot, V., Kemp, W. M., Ulloa, O., Elmgren, R., Escobar-Briones, E., and Van der Plas, A. K. (2010). Natural and human-induced hypoxia and consequences for coastal areas : Synthesis and future development. *Biogeosciences*, *7*(5), 1443-1467. https://doi.org/10.5194/bg-7-1443-2010

Zhu, M.-X., Liu, J., Yang, G.-P., Li, T., and Yang, R.-J. (2012). Reactive iron and its buffering capacity towards dissolved sulfide in sediments of Jiaozhou Bay, China. *Marine Environmental Research*, *80*, 46-55. https://doi.org/10.1016/j.marenvres.2012.06.010